西天山小哈拉军山富钛磁铁矿辉长岩的岩石成因及其构造环境*

贺鹏丽[1] 黄小龙[1**] 杨帆[1] 王雪[2] 李武显[1]

HE PengLi[1], HUANG XiaoLong[1**], YANG Fan[1], WANG Xue[2] and LI WuXian[1]

1. 中国科学院广州地球化学研究所,同位素地球化学国家重点实验室,广州 510640

2. 山东科技大学地球科学与工程学院,青岛 266590

1. *State Key Laboratory of Isotope Geochemistry*, *Guangzhou Institute of Geochemistry*, *Chinese Academy of Sciences*, *Guangzhou* 510640, *China*

2. *College of Earth Science and Engineering*, *Shandong University of Science and Technology*, *Qingdao* 266590, *China*

2020-02-11 收稿, 2020-05-17 改回.

He PL, Huang XL, Yang F, Wang X and Li WX. 2020. Petrogenesis and tectonic setting of the Xiaohalajunshan titanomagnetite-rich gabbro, Western Tianshan Orogen. *Acta Petrologica Sinica*, 36(7):2001 – 2016, doi:10.18654/1000-0569/2020.07.05

Abstract The dispute of tectonic evolution of the Tianshan Orogenic Belt in the Late Paleozoic is partly due to poor understanding of the petrogenesis and tectonic setting of coeval magmatic rocks. In this study, we reported systematic petrology, mineralogy, geochemistry, and chronology data for the Xiaohalajunshan gabbro in the Western Tianshan Orogen, in order to investigate its petrogenesis, mantle source, and tectonic settings. The zircon U-Pb dating results show that the Xiaohalajunshan gabbro was emplaced in the beginning of Early Permian (295 ± 3Ma). The studied samples contain abundant titanomagnetite (up to 8% on the volume), and major rock-forming minerals such as plagioclase, clinopyroxene and amphibole are all enriched in Fe and Ti, denoting a Fe-Ti rich magmatic system. Plagioclase is an earlier phase than clinopyroxene and amphibole on the petrography, and the water contents estimated from the amphibole composition are relatively low, which all suggest that primary magma for the gabbro is relatively dry. In addition, the correlation between Al and Ti contents of clinopyroxene shows an intraplate magmatic trend. Therefore, the Xiaohalajunshan gabbro was derived from an extensional tectonic setting instead of an arc system, indicating the Western Tianshan was in a post-orogenic extensional setting at least since the beginning of Early Permian. On the other hand, the Xiaohalajunshan gabbro is enriched in large ion lithophile elements (LILE) and light rare earth elements (LREE) and relatively depleted in heavy rare earth elements (HREE) and high field strength elements (HFSE), together with its slightly positive $\varepsilon_{Nd}(t)$ value (2.34 ~ 3.30) and variable initial $^{87}Sr/^{86}Sr$ ratio (0.7045 ~ 0.7067), which indicates an enriched mantle source refertilized by the fluids from subducted oceanic plate. During the Early Permian, the Western Tianshan in a post-orogenic extensional setting is a weakened area within the Tarim large igneous province, and thus is in favor to the expression of mantle plume activities. As the Xiaohalajunshan gabbro and nearby Haladala V-Ti magnetite-rich layered gabbro show similar magma source and mineralization characteristics with closely spatial and temporal relationship, we proposed that both of them were products of the Tarim mantle plume in Early Permian.

Key words Gabbro; Titanomagnetite; Iron-rich magma; Mantle plume; Western Tianshan Orogen

摘 要 天山造山带晚古生代构造争议部分源于对晚古生代岩浆岩的岩石成因及其构造环境认识不足。本文对西天山小哈拉军山辉长岩进行了系统的矿物学、岩石学、地球化学和年代学研究,以探讨其岩石成因、地幔源区特征及其形成的构造背景。锆石 U-Pb 定年分析结果显示小哈拉军山辉长岩形成于早二叠世早期(295 ± 3Ma)。该辉长岩富含钛磁铁矿(含量高达 8vol% 以上),并且主要造岩矿物如斜长石、单斜辉石、角闪石均显示出富 Fe-Ti 的特征,表明其形成于富 Fe-Ti 的岩浆体系。岩相学特征显示,小哈拉军山辉长岩的斜长石结晶早于单斜辉石和角闪石,由角闪石成分估算的岩浆水含量相对较低,暗示了

* 本文受国家自然科学基金项目(41703033、41625007)资助.

第一作者简介:贺鹏丽,女,1989 年生,博士,助理研究员,矿物学、岩石学、矿床学专业,E-mail:penglihe@gig.ac.cn

** **通讯作者**:黄小龙,男,1972 年生,研究员,岩石地球化学专业,E-mail:xlhuang@gig.ac.cn

相对干的初始岩浆体系,并且单斜辉石的 Al-Ti 含量关系显示出板内岩浆的特征,均表明该辉长岩并非岛弧岩浆产物,应形成于拉张构造环境,因此西天山地区在早二叠世早期已处于碰撞后伸展阶段。另外,该辉长岩的全岩富集大离子亲石元素和轻稀土元素,相对亏损重稀土和高场强元素,全岩 $\varepsilon_{Nd}(t)$ 略亏损(2.34 ~ 3.30),Sr 同位素比值变化较大($^{87}Sr/^{86}Sr = 0.7045 \sim 0.7067$),表明岩浆来源于富集的地幔源区,可能与造山带形成之前的俯冲板片组分的交代富集相关。由于西天山地区在早二叠世已处于造山后的伸展阶段,是塔里木大火成岩省范围内地幔柱活动最易于表现的地区,而小哈拉军山辉长岩与相邻的哈拉达拉富 V-Ti 磁铁矿层状辉长岩具有相似的岩浆源区和矿化特征,并具有密切的时空关系,很可能都为塔里木早二叠世地幔柱活动的产物。

关键词 辉长岩;钛磁铁矿;富铁岩浆;地幔柱;西天山造山带

中图法分类号 P588.124; P597.3

中亚造山带是全球最大的显生宙增生型造山带(Cawood *et al.*, 2009),由多个地质体拼贴而成,经历了漫长的演化历史,是研究大陆地壳生长以及大陆增生成矿理论的天然实验室(图 1a, Jahn *et al.*, 2006; Windley *et al.*, 2007; Kröner *et al.*, 2017)。中国天山是中亚造山带西南部重要的组成部分,出露了大量的晚古生代岩浆岩,记录了造山带晚古生代的演化过程。前人对天山造山带的碰撞拼贴的时间存在较大争议。其中,有关最后闭合的南天山洋的闭合时间,即伊犁-中天山地块和塔里木板块(图 1b)碰撞时间有不同的观点:晚泥盆世(Xia *et al.*, 2004)、晚泥盆世-早石炭世(Allen *et al.*, 1993; Charvet *et al.*, 2007; Wang *et al.*, 2011)、早-中石炭世(Biske and Seltmann, 2010; Li *et al.*, 2018; Tong *et al.*, 2018)、晚石炭世(Gao *et al.*, 2011; Han *et al.*, 2011; Han and Zhao, 2018)和晚二叠世-中三叠世(Zhang *et al.*, 2007; Xiao *et al.*, 2013)。随着研究不断深入,南天山洋闭合的主要争议集中在晚石炭世(320 ~ 300Ma)和晚二叠世-中三叠世。对高压变质岩中锆石年龄的地质意义认识不清,以及岩浆岩的地球化学性质及其形成的构造环境存在多解性是造成这种认识差异的主要原因。因此,系统研究天山造山带晚古生代岩浆岩的时空格架和岩石成因机制对深入理解其构造演化具有重要意义。

在东天山-北山地区发育丰富的二叠纪镁铁-超镁铁 Cu-Ni 硫化物矿床,如黄山、镜儿泉、大草滩、白石泉岩体等(任明浩等, 2013; Su *et al.*, 2013; Mao *et al.*, 2018),可能与塔里木早二叠世地幔柱活动相关(Qin *et al.*, 2011; Su *et al.*, 2015)。西天山晚古生代则主要发育赋存于晚石炭世火山岩沉积岩中的铁矿床或矿化现象,如智博、查岗诺尔、阔拉萨依铁矿等(Zhang *et al.*, 2012, 2015a; 高永伟等, 2017)。研究表明这些铁矿床的 Fe 经历了两阶段富集过程,早期为来源于俯冲带的岩浆经演化形成富铁岩浆,晚期通过水岩反应形成富 Fe 流体(Zhang *et al.*, 2012, 2015a; 高永伟等, 2017)。相对而言,西天山的镁铁-超镁铁质侵入岩的富 Fe 或 Cu 矿化较为罕见,但特克斯县东北部的哈拉达拉晚石炭世末期的层状辉长岩(~300Ma)发育有富钒钛磁铁矿层(图 1c, 高纪璞等, 1991; 贺鹏丽等, 2013; He *et al.*, 2016),目前可见的铁矿化规模有限。先前研究表明,哈拉达拉层状辉长岩富钒钛磁铁矿是地幔柱叠加于造山带构造背景下产生的高温、贫水、低氧逸度原始岩浆经充分结晶分异的结果(He *et al.*, 2016)。另外,前人研究发现特克斯县东南方向约 10km 的小哈拉军山辉长岩(图 1c)亦具有富钛磁铁矿岩石类型,且认为与哈拉达拉层状辉长岩可能为同期岩浆活动(郭璇和朱永峰, 2011),但并不清楚是否同样为地幔柱活动的产物,对其岩浆源区特征以及富铁的机制也未有研究。因此,本文将通过详细的矿物学、岩石学、地球化学和年代学研究,确定小哈拉军山富钛磁铁矿辉长岩的形成时代,探讨其岩浆性质、源区特征、富铁的机制及其形成的构造环境,从而为深入理解西天山晚古生代构造演化提供有用信息。

1 地质背景及其样品描述

中国天山造山带东西绵延约 1700km,沿托克逊-库米什公路分割为东、西两部分。西天山北接准噶尔盆地,南临塔里木克拉通,自北向南由北天山造山带、伊犁-中天山地块和南天山造山带组成(图 1b)。南天山造山带由塔里木克拉通和伊犁-中天山地块碰撞、南天山洋消失形成,可能代表了中亚造山带西南部增生造山活动的结束(Xiao *et al.*, 2010; Han *et al.*, 2011)。前人对南天山造山带形成时间有很大争议,主要集中在晚石炭世(Gao *et al.*, 2011; Han *et al.*, 2011; Klemd *et al.*, 2015; Alexeiev *et al.*, 2019)和晚二叠世-中三叠世(Xiao *et al.*, 2013; Xiao and Santosh, 2014)两种认识。北天山造山带由蛇绿岩和高压变质岩带及古生代火山-沉积地层和岩浆岩组成,属于伊犁-中天山地块和准噶尔盆地碰撞拼贴、北天山洋闭合形成的岩浆弧。伊犁-中天山是哈萨克斯坦微陆块向东延伸的部分,其含有前寒武纪基底及古生代火山-沉积盖层。前寒武纪变质岩和沉积岩的锆石年龄结果显示,伊犁-中天山前寒武纪基底年龄变化很大,从中太古代(~2.8Ga)至新元古代(~0.8Ga)均有出现,但其峰值年龄为 1.4 ~ 1.8Ga 和 0.8 ~ 1.2Ga(Wang *et al.*, 2014; Gao *et al.*, 2015; He *et al.*, 2015; Huang *et al.*, 2016; Zhu *et al.*, 2019)。伊犁-中天山出露南北两条古生代岩浆带,分别属于南天山洋和北天山洋向伊犁-中天山俯冲形成的弧火山岩,主要形成于志留纪到早石炭世,并叠加了晚石炭世-二叠纪火山沉积岩和侵入岩(龙灵利等, 2007; Gao *et al.*, 2009; Han *et al.*, 2010; Zhang *et al.*, 2015b; He *et al.*, 2016)。

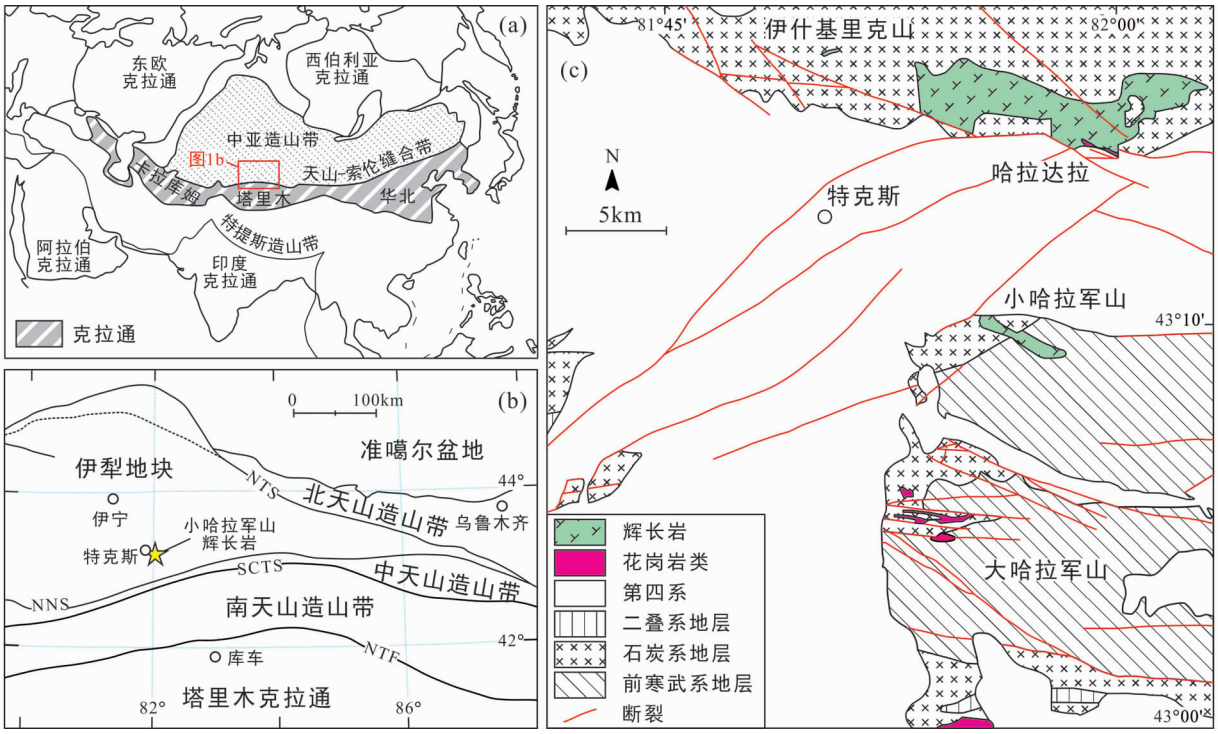


图 1 小哈拉军山辉长岩位置

(a)中亚造山带及其周边主要克拉通和造山带位置简图(据Şengör *et al.*, 1993 修改);(b)中国西天山造山带及其邻区构造简图(据 Qian *et al.*, 2009 修改),NTS-北天山缝合带,NNS-尼古拉耶夫线-那拉提北缘缝合带,SCTS-中天山南缘缝合带,NTF-塔里木北缘断裂;(c)小哈拉军山辉长岩及邻区地质简图(据新疆地质局区域地质调查队, 1975～1979①)

Fig. 1 Location of the Xiaohalajunshan gabbro

(a) simplified geologic map of the Central Asian Orogenic Belt and peripheral major cratons and orogenic belts (modified after Şengör *et al.*, 1993); (b) simplified tectonic map of Chinese Western Tianshan Orogen and adjacent area (modified after Qian *et al.*, 2009), NTS-North Tianshan Suture, NNS-Nikolaev Line-North Nalati Suture, SCTS-South Central Tianshan Suture, NTF-North Tianshan Fault; (c) simplified geologic map of the Xiaohalajunshan gabbro and its adjacent region

小哈拉军山辉长岩位于特克斯县城东南方向约 10km 处(图 1c)。岩体在平面上呈 NW-SE 向的长条状展布,出露面积约 5km^2。岩体侵入到北面的石炭系火山-沉积地层和南面的前寒武系地层中。小哈拉军山辉长岩呈辉长-辉绿结构和似斑状构造,主要组成矿物为斜长石(40% ～60%)、单斜辉石(10% ～30%)、角闪石(10% ～30%)和磁铁矿(4% ～10%),少量为黑云母、榍石、磷灰石等。斜长石呈自形柱状,颗粒大小变化较大,具有明显的环带结构,边部常包裹自形粒状磁铁矿,部分泥化或绢云母化(图 2)。单斜辉石多呈破碎状,常包裹磁铁矿,部分绿泥石化或碳酸盐化(图 2a-c)。角闪石较为新鲜,常呈半自形-他形破碎状,包裹磁铁矿(图 2a, b)。磁铁矿呈自形粒状,大部分呈间隙矿物充填于斜长石格架中,但少数呈包裹体包裹于其他矿物(图 2)。碳酸盐具有明显的次生成因特征,呈不规则状,并且与其他次生矿物(如绿泥石)共生,部分呈碳酸盐脉(图 2c, d)。本次研究对 9 块岩石样品进行了矿物成分和全岩地球化学主、微量元素及 Sr-Nd 同位素分析,并对样品 TKS89 进行了锆石 U-Pb 年龄分析。

2 分析方法

本文涉及的分析测试均在中国科学院广州地球化学研究所同位素地球化学国家重点实验室完成。

锆石 U-Pb 年龄由 CAMECA IMS-1280 二次离子质谱仪(SIMS)测定,详细的分析方法参见 Li *et al.* (2010),测定的监控标样 Qinghu 锆石的 U-Pb 谐和年龄为 161 ±2Ma(2σ, n =6,推荐值 159.5 ±0.2Ma,Li *et al.*, 2013)。

全岩主量元素数据采用 Rigaku RIX 100e 型 X 射线荧光光谱仪(XRF)测定,元素分析精度优于 1% ～5%。微量元素数据采用 Perkin-Elmer Sciex ELAN 6000 型电感耦合等离子质谱仪(ICP-MS)分析,绝大多数元素的分析精度为 1% ～5%。全岩 Sr-Nd 同位素采用 Neptune Plus 多接收电感耦合等离子质谱仪(MC-ICP-MS)测定,流程监控标样 BHVO-2 的

① 新疆地质局区域地质调查队. 1975～1979. 1∶20 万昭苏幅地质图



图 2 小哈拉军山辉长岩的岩相学特征

(a)半自形-他形的单斜辉石(Cpx)和角闪石(Am)充填在自形的斜长石(Pl)格架中,斜长石部分泥化,磁铁矿(Mag)包裹在单斜辉石和角闪石中,磁铁矿占比约 8%(正交偏光);(b)部分细粒磁铁矿包裹在半自形-他形的角闪石中,磁铁矿占比约 4%,单斜辉石发生绿泥石化,(单偏光);(c)粗粒斜长石具有环带结构,边部包裹自形粒状磁铁矿,磁铁矿占比约 2%,次生碳酸盐(Cal)呈他形充填(正交偏光);(d)辉绿结构,镁铁质矿物多发生碳酸盐化或绿泥石化,可见碳酸盐脉,磁铁矿占比约 6%,但斜长石核部未见磁铁矿包裹体(正交偏光)

Fig. 2 Petrography of the Xiaohalajunshan gabbro

(a) subhedral-anhedral clinopyroxene (Cpx) and amphibole (Am) are interstitial phases between euhedral plagiolcase (Pl); plagioclase is partially pelitized; some magnetites (Mag) are enclosed in clinopyroxene and amphibole; magnetite is ~8% in this thin-section (crossed-polarized light); (b) some small-grained magnetites are enclosed in subhedral-anhedral amphibole; magnetite is ~4% in this thin-section; clinopyroxene has been altered to chlorite (plane-polarized light); (c) coarse-grained plagioclase shows zoning texture and has euhedral magnetite inclusions in the rim; magnetite is ~2% in this thin-section; the secondary carbonate is irregular in shape (crossed-polarized light); and (d) some sample show ophitic texture; mafic minerals are usually altered into carbonatization or chloritization, and carbonate veins are common; magnetite is ~6% in this thin-section but magnetite inclusion is absent in the core of plagioclases (crossed-polarized light)

Sr-Nd 同位素含量分别为 $^{87}Sr/^{86}Sr = 0.703503 \pm 0.000011$, $^{143}Nd/^{144}Nd = 0.512993 \pm 0.000006$,仪器监控标样 NBS987 的 $^{87}Sr/^{86}Sr = 0.710267 \pm 16$(n = 6,95% 的置信区间),Jndi-1 的 $^{143}Nd/^{144}Nd = 0.512115 \pm 6$(n = 4,95% 的置信区间),与推荐值 0.512115 ± 5(Tanaka *et al.*, 2000)一致。详细的样品前处理及实验测试方法参见 He *et al.* (2016)。

矿物电子探针成分分析及其背散射电子图像使用 CAMECA SX-Five 场发射电子探针完成。定量分析工作条件为:加速电压 15kV,探针电流 20nA,束斑直径 2~5μm,采用 PAP(Pouchou & Pichoir)修正法进行基体校正(Pouchou and Pichoir, 1991)。根据元素强度和性质不同,元素峰位分析时间选择 8~120s 之间,单侧背景时间为峰位时间的一半。分析过程采用美国 SPI 公司的硅酸盐矿物或氧化物作为标样,高含量元素检测限为 $100 \times 10^{-6} \sim 300 \times 10^{-6}$,微量元素的检测限优于 100×10^{-6}。

3 分析结果

3.1 锆石 U-Pb 年龄

小哈拉军山辉长岩样品 TKS89 的锆石数量较少,且颗粒较小,呈破碎的短柱状,长边从 50μm 到小于 20μm 变化,可能是由于样品前处理过程中过度破碎造成。锆石的 CL 图像呈现出清晰且较宽的振荡环带,其 Th、U 含量变化较大(分别为 $40 \times 10^{-6} \sim 803 \times 10^{-6}$, $111 \times 10^{-6} \sim 1161 \times 10^{-6}$),具有较高的 Th/U 比值(Th/U = 0.14~2.81,表 1),表明为岩浆成因锆石。其中,1、3、8 和 10 号分析点的 $^{206}Pb/^{238}U$ 年龄明显老于其他分析点,并且变化范围较大(2322~840Ma),显示继承锆石的特征,在伊犁-中天山地块前寒武纪变质基底的年龄范围(0.8~2.8Ga)。另外,12 号分析点具有最低的 $^{206}Pb/^{204}Pb$ 比值,其普通 Pb 比例明显较高,因而产生较大的 $^{206}Pb/^{238}U$ 年龄校正误差。其他的 11 个分析点具有相近的

表 1 小哈拉军山辉长岩锆石 SIMS U-Pb 定年分析结果

Table 1 Zircon SIMS U-Pb dating results for the Xiaohalajunshan gabbro

测点号	U ($\times10^{-6}$)	Th ($\times10^{-6}$)	Th/U	$^{206}Pb/^{204}Pb$	f_{206} (%)	同位素比值			同位素年龄(Ma)			协和度 (%)
						$^{207}Pb/^{206}Pb$	$^{207}Pb/^{235}U$	$^{206}Pb/^{238}U$	$^{207}Pb/^{206}Pb$	$^{207}Pb/^{235}U$	$^{206}Pb/^{238}U$	
#1	160	91	0.57	3906	0.48	0.1498 ± 7	8.9594 ± 1679	0.4337 ± 78	2344 ± 8	2334 ± 17	2322 ± 35	100
#2	140	161	1.15	1148	1.63	0.0551 ± 37	0.3688 ± 256	0.0485 ± 9	418 ± 143	319 ± 19	305 ± 5	104
#3	1042	147	0.14	1268	1.48	0.0699 ± 44	1.3418 ± 871	0.1391 ± 25	927 ± 123	864 ± 39	840 ± 14	103
#4	111	115	1.03	1011	1.85	0.0570 ± 45	0.3815 ± 307	0.0485 ± 9	492 ± 164	328 ± 23	305 ± 5	107
#5	184	166	0.90	1139	1.64	0.0522 ± 22	0.3339 ± 153	0.0464 ± 8	296 ± 93	293 ± 12	292 ± 5	100
#6	581	405	0.70	1683	1.11	0.0521 ± 10	0.3383 ± 89	0.0471 ± 8	291 ± 43	296 ± 7	296 ± 5	100
#7	414	415	1.00	827	2.26	0.0554 ± 25	0.3619 ± 177	0.0474 ± 9	427 ± 98	314 ± 13	299 ± 5	105
#8	285	803	2.81	3386	0.55	0.0948 ± 9	3.4159 ± 699	0.2613 ± 47	1525 ± 18	1508 ± 16	1496 ± 24	101
#9	694	445	0.64	923	2.03	0.0527 ± 13	0.3442 ± 103	0.0474 ± 9	317 ± 53	300 ± 8	298 ± 5	101
#10	112	40	0.36	1101	1.70	0.1480 ± 11	7.7676 ± 1532	0.3806 ± 69	2323 ± 13	2204 ± 18	2079 ± 32	106
#11	595	311	0.52	2361	0.79	0.0535 ± 22	0.3408 ± 154	0.0462 ± 8	349 ± 91	298 ± 12	291 ± 5	102
#12	1161	652	0.56	261	7.17	0.0538 ± 99	0.0420 ± 77	0.0057 ± 1	363 ± 369	42 ± 8	36 ± 1	115
#13	471	285	0.60	1640	1.14	0.0502 ± 22	0.3223 ± 154	0.0466 ± 8	205 ± 100	284 ± 12	293 ± 5	97
#14	206	145	0.70	546	3.43	0.0507 ± 53	0.3195 ± 338	0.0457 ± 8	229 ± 224	282 ± 26	288 ± 5	98
#15	654	366	0.56	3092	0.60	0.0566 ± 20	0.3593 ± 142	0.0461 ± 8	475 ± 76	312 ± 11	290 ± 5	107
#16	417	243	0.58	3073	0.61	0.0587 ± 28	0.3695 ± 187	0.0456 ± 8	558 ± 100	319 ± 14	288 ± 5	111

注：f_{206} 表示普通 ^{206}Pb 占测量的 ^{206}Pb 比例

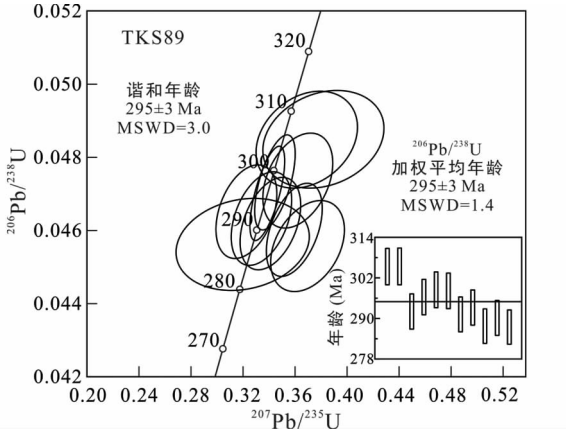


图 3 小哈拉军山辉长岩锆石 SIMS U-Pb 年龄

Fig. 3 Zircon SIMS U-Pb age for the Xiaohalajunshan gabbro

$^{206}Pb/^{238}U$ 年龄(288 ± 5Ma ~ 305 ± 5Ma)，所得的 U-Pb 谐和年龄(295 ± 3Ma；2σ)与加权平均$^{206}Pb/^{238}U$ 年龄(295 ± 3Ma；2σ)一致(图 3)，代表了小哈拉军山辉长岩的形成年龄，与特克斯县城东北部同样侵入到石炭系中的哈拉达拉含钒钛磁铁矿层状辉长岩的形成年龄(300 ± 1Ma；He *et al.*，2016)一致。

3.2 全岩主、微量元素及 Sr-Nd 同位素特征

小哈拉军山辉长岩的 SiO_2(45.64% ~ 47.97%)、Al_2O_3(16.06% ~ 17.05%)、TiO_2(1.87% ~ 2.12%)变化较小，而 CaO(6.26% ~ 10.28%)变化较大(表 2)。其 MgO(3.77% ~ 5.89%)含量较低，$Fe_2O_3{}^T$(10.29% ~ 11.88%)含量较高，因而具有较低的 $Mg^{\#}$($Mg/(Mg+Fe^T)\times100\%$ = 42 ~ 51)值(表 2)。K_2O 含量为 0.55% ~ 1.70%，属于钙碱性-高 K 钙碱性系列岩石；另外，其 Na_2O 含量较高(3.11% ~ 4.83%)，因此具有较低的 K_2O/Na_2O 比值(0.18 ~ 0.40)；总碱含量中等，属于亚碱性玄武岩系列。样品的烧失量较高(4.00% ~ 6.73%)，但是除了 Rb、Ba、Pb 变化较大外，其他微量元素均协同变化，各样品具有一致的稀土元素配分曲线和微量元素蛛网图(图 4)。小哈拉军山辉长岩的稀土元素总量较高(111×10^{-6} ~ 145×10^{-6})，但相对于 OIB(Sun and McDonough，1989)其轻、重稀土分异较弱(La/Yb = 6.05 ~ 7.66)，没有明显的 Eu 异常($\delta Eu = 0.98 \sim 1.06$)(图 4)。微量元素蛛网图中显示出明显的 Nb、Ta 负异常以及轻微的 Zr、Hf 负异常和 Sr 正异常，但未见明显的 Ti 异常(图 4)。所分析样品的 Cr(31.0×10^{-6} ~ 75.9×10^{-6})和 Ni(23.9×10^{-6} ~ 44.0×10^{-6})含量相对较低，但 V 含量较高(200×10^{-6} ~ 243×10^{-6})。

小哈拉军山辉长岩的$^{87}Sr/^{86}Sr$ 初始比值变化相对较大(0.7045 ~ 0.7067)，而$^{143}Nd/^{144}Nd$ 初始比值变化较小，具有正的 $\varepsilon_{Nd}(t)$值(2.34 ~ 3.30)(表 3、图 5)，相对于哈拉达拉层状辉长岩显示出略为富集的 Nd 同位素特征(图 5)。

表 2 小哈拉军山辉长岩全岩主要氧化物(wt%)和微量元素($\times 10^{-6}$)含量分析结果

Table 2 Major oxides (wt%) and trace elements ($\times 10^{-6}$) contents for the Xiaohalajunshan gabbro

样品号	TKS50	TKS51	TKS52	TKS53	TKS54	TKS55	TKS88	TKS89	TKS90
SiO_2	46.98	46.09	47.25	47.31	45.64	47.16	45.74	47.97	47.01
TiO_2	1.98	1.92	1.99	2.00	1.88	2.12	1.87	1.90	1.91
Al_2O_3	17.01	16.84	16.59	16.24	17.05	16.06	16.96	16.20	16.59
$Fe_2O_3^T$	11.16	11.04	11.27	11.27	10.84	11.88	10.29	10.94	11.43
MnO	0.14	0.16	0.14	0.14	0.14	0.16	0.11	0.17	0.16
MgO	4.54	4.86	4.57	4.71	4.40	5.01	3.77	5.03	5.89
CaO	8.95	8.76	7.98	8.55	9.82	6.26	10.28	6.80	6.27
Na_2O	3.47	3.18	3.74	3.44	3.11	4.83	3.22	4.28	4.16
K_2O	0.72	0.57	1.09	0.72	0.55	1.47	0.68	1.70	1.40
P_2O_5	0.44	0.43	0.49	0.53	0.42	0.50	0.42	0.47	0.41
LOI	4.25	6.02	4.92	5.01	5.93	4.00	6.73	4.21	4.36
Total	99.64	99.89	100.03	99.91	99.76	99.43	100.07	99.68	99.58
$Mg^{\#}$	44.6	46.6	44.6	45.3	44.5	45.5	42.1	47.7	50.5
Sc	25.5	23.1	24.5	23.6	22.6	25.6	24.6	23.9	23.9
V	235	226	223	225	226	243	217	201	218
Cr	67.2	46.6	46.0	47.4	75.9	52.0	46.5	31.0	45.9
Co	42.1	35.3	39.4	35.8	38.0	39.2	40.2	40.3	43.0
Ni	37.9	31.6	31.8	30.0	44.0	29.3	32.8	23.9	33.1
Cu	41.9	36.4	41.8	32.8	41.8	43.7	40.5	33.8	42.3
Zn	108	102	112	114	89.1	101	130	100	95.9
Ga	19.5	18.3	18.5	19.7	18.3	18.6	18.6	18.8	18.0
Ge	2.88	2.70	2.79	2.98	2.59	2.87	2.62	2.92	3.28
Rb	17.7	12.5	41.7	18.7	13.2	54.8	21.8	56.6	45.0
Sr	592	609	639	593	585	588	593	546	622
Y	29.8	26.1	29.6	32.8	26.9	32.0	26.9	28.0	24.5
Zr	203	177	185	218	151	202	172	191	165
Nb	10.5	10.0	10.8	12.3	9.01	11.0	8.95	10.9	8.87
Cs	1.54	1.55	1.77	1.49	2.35	2.70	3.03	1.39	1.37
Ba	270	254	528	296	199	486	225	380	404
La	17.9	17.6	19.9	22.0	16.1	19.4	17.5	20.9	16.3
Ce	43.0	41.9	47.1	53.0	39.0	47.0	42.7	49.3	39.4
Pr	6.12	5.75	6.49	7.38	5.57	6.54	5.93	6.76	5.44
Nd	27.0	25.1	28.2	31.1	24.3	28.5	26.5	30.2	24.3
Sm	5.97	5.51	6.23	6.97	5.44	6.36	5.93	6.57	5.51
Eu	1.90	1.79	2.05	2.22	1.88	2.07	1.93	2.07	1.81
Gd	5.62	5.13	5.90	6.48	5.18	6.12	5.61	6.06	5.18
Tb	0.95	0.84	0.97	1.07	0.88	1.02	0.91	0.97	0.85
Dy	5.53	4.91	5.57	6.17	5.07	5.89	5.31	5.58	5.01
Ho	1.12	0.99	1.10	1.24	1.02	1.19	1.07	1.10	0.99
Er	3.09	2.66	3.05	3.36	2.69	3.29	2.87	3.03	2.67
Tm	0.45	0.40	0.45	0.50	0.42	0.48	0.42	0.43	0.40
Yb	2.96	2.57	2.88	3.22	2.59	3.11	2.59	2.72	2.42
Lu	0.46	0.40	0.45	0.50	0.40	0.49	0.39	0.41	0.37
Hf	4.36	3.86	4.09	4.73	3.59	4.44	3.91	4.32	3.83
Ta	0.57	0.51	0.55	0.64	0.49	0.58	0.52	0.60	0.50
Pb	7.12	6.63	8.51	8.05	3.44	7.26	13.4	4.11	5.54
Th	1.86	1.79	1.94	2.28	1.44	1.87	1.64	2.05	1.58
U	0.41	0.37	0.40	0.48	0.31	0.40	0.39	0.43	0.37
La/Yb	6.05	6.83	6.91	6.83	6.21	6.23	6.77	7.66	6.71
Nb/U	25.7	26.9	27.0	25.6	28.9	27.7	23.1	25.1	24.2
∑REE	122	116	130	145	111	131	120	136	111
δEu	0.99	1.01	1.02	0.99	1.06	1.00	1.01	0.98	1.02

注:LOI 为烧失量;$Mg^{\#} = Mg/(Mg + Fe^T) \times 100\%$,$Fe_2O_3^T$ 为以 Fe_2O_3 表示全铁的氧化物;$\delta Eu = 2 \times Eu_N/(Sm_N + Gd_N)$,N 为球粒陨石标准化

表 3 小哈拉军山辉长岩全岩 Sr-Nd 同位素分析结果

Table 3 Sr-Nd isotopic data for the Xiaohalajunshan gabbro

样品号	TKS50	TKS51	TKS52	TKS54	TKS88	TKS89	TKS90
$^{87}Sr/^{86}Sr$	0.705535	0.705629	0.705282	0.705311	0.705739	0.707099	0.707535
2σ	0.000010	0.000010	0.000011	0.000012	0.000010	0.000012	0.000010
$(^{87}Sr/^{86}Sr)_i$	0.7052	0.7054	0.7045	0.7050	0.7053	0.7058	0.7067
$^{143}Nd/^{144}Nd$	0.512685	0.512634	0.512651	0.512678	0.512683	0.512644	0.512671
2σ	0.000004	0.000006	0.000007	0.000005	0.000006	0.000005	0.000005
$\varepsilon_{Nd}(t)$	3.30	2.34	2.62	3.10	3.19	2.57	2.89
t_{DM}(Ga)	0.89	0.97	0.95	0.92	0.91	0.94	0.95

注：$^{87}Rb/^{86}Sr$ 和 $^{147}Sm/^{144}Nd$ 由表 2 全岩 Rb、Sr、Sm 和 Nd 含量计算；$^{87}Sr/^{86}Sr$ 和 $^{143}Nd/^{144}Nd$ 的误差均为 2σ；$\varepsilon_{Nd}(t)=[(^{143}Nd/^{144}Nd)_S/(^{143}Nd/^{144}Nd)_{CHUR}-1]\times10000$；$(^{143}Nd/^{144}Nd)_{CHUR}=0.512638$，$t=295$Ma

表 4 单斜辉石代表性电子探针分析结果(wt%)

Table 4 Representative electron probe analyses of clinopyroxenes from the Xiaohalajunshan gabbro (wt%)

测点号	#1	#2	#3	#4	#5	#6	#7	#8	#9
SiO_2	50.82	47.63	49.31	49.02	47.25	48.08	47.63	47.29	46.56
TiO_2	1.31	2.35	1.73	1.63	2.41	2.01	1.90	2.50	2.60
Al_2O_3	2.97	5.63	4.14	4.01	5.83	5.15	5.26	5.84	6.60
Cr_2O_3	0.03	0.03	0.00	0.01	0.01	0.00	0.02	0.01	0.01
FeO^T	8.26	9.45	8.76	8.38	9.12	9.48	8.99	9.21	9.23
MnO	0.25	0.22	0.25	0.21	0.20	0.20	0.15	0.20	0.21
MgO	14.90	12.81	13.64	13.61	12.72	12.90	12.82	12.98	12.76
CaO	20.75	21.16	21.26	21.56	21.18	21.02	21.24	21.43	21.04
Na_2O	0.36	0.51	0.52	0.48	0.55	0.54	0.53	0.47	0.49
Total	99.66	99.80	99.63	98.91	99.28	99.40	98.54	99.94	99.50
En	44.2	40.4	42.0	42.1	40.6	40.7	40.8	41.0	40.9
Wo	44.3	48.0	47.1	47.9	48.6	47.6	48.6	48.7	48.5
Fs	11.5	11.5	10.9	10.0	10.9	11.7	10.6	10.3	10.5
Al_R^{IV}	5.5	10.9	8.0	7.9	11.3	9.8	10.0	11.7	12.7
$Mg^{\#}$	76.3	70.7	73.5	74.3	71.3	70.8	71.8	71.5	71.1
Fe^{2+}/Fe^T	0.83	0.69	0.72	0.69	0.67	0.70	0.66	0.63	0.63

注：Al_R^{IV} 为 Al 在四次配位阳离子位置占位比例；$Mg^{\#}=Mg/(Mg+Fe^T)\times100\%$，$FeO^T$ 为以 FeO 表示全铁的氧化物

3.3 矿物成分

3.3.1 单斜辉石

小哈拉军山辉长岩中的单斜辉石成分较均匀，MgO 较低(12.72% ~14.90%)，FeO^T 相对较高(8.26% ~9.48%)，因此 $Mg^{\#}$较低(71 ~76)(表 4)，端元成分为 $Wo_{44.3\text{-}48.7}En_{40.4\text{-}44.2}Fs_{10.0\text{-}11.7}$，属于透辉石-次透辉石系列。另外，单斜辉石的 Na_2O 含量较低(0.36% ~0.55%)，TiO_2 含量较高(1.31% ~2.60%)，Al_2O_3 含量变化较大(2.97% ~6.60%)。

3.3.2 角闪石

角闪石成分变化较大，主要为镁绿钙闪石。角闪石的 Al_2O_3 含量变化较大(6.83% ~11.10%)，并具有高 TiO_2(2.11% ~4.45%)和低 $Mg^{\#}$(53 ~68)的特征(表 5)。

3.3.3 斜长石

粗粒斜长石显示出明显的韵律环带或正环带的结构特征，细粒斜长石具有正环带结构特征。斜长石成分变化较大($An_{20.1\text{-}69.2}Ab_{30.1\text{-}76.2}Or_{0.7\text{-}4.9}$)，属于奥长石-培长石范围，以拉长石为主，粗粒斜长石边部和细粒斜长石具有奥长石-中长石成分(表 6)。斜长石的 FeO^T 含量变化很大(0.28% ~0.81%)，与 An 呈较好的正相关关系。

3.3.4 磁铁矿

磁铁矿中 FeO^T(63.49% ~85.32%)、TiO_2(5.20% ~23.30%)和 V_2O_3 含量(0.17% ~0.65%)含量变化较大，属于钛磁铁矿。钛磁铁矿成分变化范围主要为 TiO_2 = 17% ~20%和 FeO^T = 70% ~74%，并具有较高的 V_2O_3 含量(0.50% ~0.65%)(表 7)，略低于峨眉山基性-超基性钒钛

表 5 角闪石代表性电子探针分析结果(wt%)

Table 5 Representative electron probe analyses of amphiboles from the Xiaohalajunshan gabbro (wt%)

测点号	#1	#2	#3	#4	#5	#6	#7	#8	#9	#10	#11
SiO_2	45.20	41.82	43.84	42.38	45.61	42.05	43.93	41.74	42.48	46.12	43.64
TiO_2	2.11	3.86	3.27	3.86	2.51	4.45	3.20	4.28	4.11	2.73	3.20
Al_2O_3	8.24	10.86	8.86	9.52	7.76	10.71	8.78	11.10	10.42	6.83	9.15
FeO^T	14.57	13.69	14.56	17.20	13.64	12.47	14.50	12.33	11.78	14.84	12.05
MnO	0.34	0.27	0.31	0.47	0.33	0.27	0.34	0.24	0.23	0.39	0.29
MgO	13.42	12.66	12.67	10.86	14.11	13.41	12.78	13.33	13.68	13.60	14.60
CaO	10.20	10.89	10.25	9.86	10.43	10.92	10.21	11.05	10.98	9.72	10.32
Na_2O	3.01	3.07	3.23	3.09	3.00	2.93	2.90	2.94	3.06	3.00	3.13
F	0.26	0.34	0.23	0.43	0.58	0.24	0.07	0.18	0.20	0.12	0.47
Cl	0.04	0.02	0.03	0.04	0.04	0.02	0.04	0.03	0.02	0.04	0.03
Total	97.39	97.48	97.24	97.70	98.01	97.47	96.75	97.21	96.95	97.39	96.85
H_2O_m	4.85	5.90	4.83	5.75	4.40	4.06	3.40	4.49	4.03	2.87	2.88
ΔNNO	0.0	0.1	0.0	0.0	0.0	0.0	0.0	0.1	0.1	0.0	0.0
$Mg^{\#}$	62.1	62.2	60.8	53.0	64.8	65.7	61.1	65.8	67.4	62.0	68.4

注:H_2O_m 为平衡熔体的 H_2O;$Mg^{\#} = Mg/(Mg + Fe^T) \times 100\%$;$FeO^T$ 为以 FeO 表示全铁的氧化物;NNO 为镍-氧化镍

表 6 斜长石代表性电子探针分析结果(wt%)

Table 6 Representative electron probe analyses of plagioclases from the Xiaohalajunshan gabbro (wt%)

测点号	#1	#2	#3	#4	#5	#6	#7	#8	#9	#10	#11
SiO_2	53.37	63.14	53.68	52.53	56.24	61.74	50.30	52.09	54.67	54.31	55.41
Al_2O_3	29.15	23.31	28.73	29.50	27.33	24.60	30.68	28.77	28.69	30.36	27.33
FeO^T	0.42	0.29	0.58	0.55	0.39	0.28	0.56	0.81	0.55	0.66	0.50
CaO	11.71	4.23	11.29	12.30	9.49	5.80	13.71	12.11	9.59	11.94	9.95
Na_2O	4.61	8.89	4.77	4.18	5.89	8.05	3.30	4.28	4.71	4.05	5.48
K_2O	0.17	0.66	0.18	0.15	0.23	0.43	0.11	0.15	0.78	0.17	0.26
Total	99.43	100.52	99.23	99.21	99.58	100.91	98.67	98.21	98.99	101.50	98.94
An	57.8	20.1	56.1	61.3	46.5	27.8	69.2	60.5	50.4	61.3	49.3
Ab	41.2	76.2	42.8	37.7	52.2	69.8	30.1	38.6	44.8	37.6	49.1
Or	1.0	3.7	1.1	0.9	1.4	2.5	0.7	0.9	4.9	1.0	1.5

注:FeO^T 为以 FeO 表示全铁的氧化物

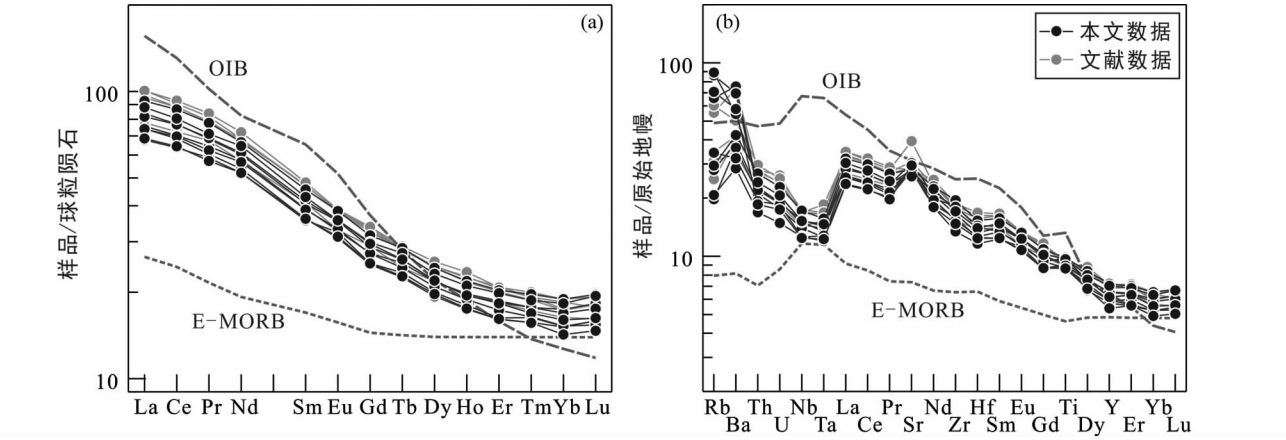


图 4 小哈拉军山辉长岩全岩球粒陨石标准化稀土元素配分曲线(a)及原始地幔标准化微量元素蛛网图(b)

OIB、E-MORB、球粒陨石和原始地幔值均来自 Sun and McDonough (1989). 文献数据来自郭璇和朱永峰(2011),图 6 同

Fig. 4 Chondrite-normalized REE patterns (a) and primitive mantle-normalized multi-element diagrams (b) for the Xiaohalajunshan gabbro

The OIB, E-MORB, chondrite and primitive mantle date are all from Sun and McDonough (1989). Literature data from Guo and Zhu (2011), also in Fig. 6

表 7 钛磁铁矿代表性电子探针分析结果(wt%)

Table 7 Representative electron probe analyses of titanomagnetite from the Xiaohalajunshan gabbro (wt%)

测点号	#1	#2	#3	#4	#5	#6	#7	#8	#9	#10	#11
SiO_2	0.46	0.13	0.70	0.05	0.11	0.07	2.26	0.12	1.13	1.14	0.10
TiO_2	17.93	18.84	18.22	18.21	19.06	18.37	14.91	17.73	5.20	23.30	19.23
Al_2O_3	1.71	1.47	1.44	2.28	2.84	0.89	0.79	1.13	0.08	1.24	0.78
Cr_2O_3	0.15	0.19	0.15	0.10	0.24	0.24	0.39	1.02	0.04	0.21	0.11
V_2O_3	0.57	0.65	0.64	0.59	0.61	0.55	0.54	0.55	0.17	0.63	0.59
FeO^T	71.65	70.76	70.51	71.18	69.92	73.37	72.67	72.92	85.32	63.49	72.76
MnO	0.15	0.07	0.59	0.09	0.12	0.27	0.11	0.20	0.13	0.87	0.20
MgO	bdl	bdl	0.03	0.02	0.03	bdl	0.15	bdl	0.01	0.04	0.02
CaO	0.59	0.18	0.67	0.23	0.09	0.10	1.66	0.04	0.55	1.37	0.12
Total	93.21	92.29	92.97	92.74	93.03	93.86	93.49	93.71	92.63	92.30	93.91

注：FeO^T 为以 FeO 表示全铁的氧化物；bdl 为低于检测限

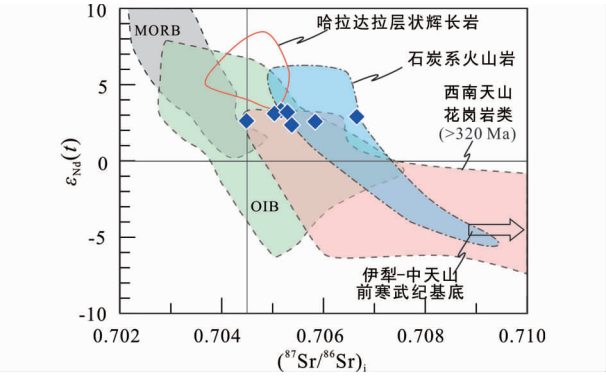


图 5 小哈拉军山辉长岩全岩 $(^{87}Sr/^{86}Sr)_i$-$\varepsilon_{Nd}(t)$ 图解

文献数据来源：伊犁-中天山前寒武纪基底(Long *et al.*, 2011; Xiong *et al.*, 2019)；西南天山花岗岩类(>320Ma)(Gao *et al.*, 2009; Long *et al.*, 2011; Gou *et al.*, 2012 及其相关文献)；石炭纪火山岩(Zhu *et al.*, 2009; Ge *et al.*, 2015)；哈拉达拉层状辉长岩(龙灵利等, 2012; He *et al.*, 2016). MORB 和 OIB 范围据 Huang *et al.* (2012)

Fig. 5 The diagram of $(^{87}Sr/^{86}Sr)_i$ vs. $\varepsilon_{Nd}(t)$ for the Xiaohalajunshan gabbro

Sr-Nd isotopic data sources: Yili-Central Tianshan Precambrian granitic gneisses (Long *et al.*, 2011; Xiong *et al.*, 2019); Paleozoic granites (>320Ma) in Southwest Tianshan (Gao *et al.*, 2009; Long *et al.*, 2011; Gou *et al.*, 2012, and reference therein); Carboniferous volcanic sedimentary sequence (Zhu *et al.*, 2009; Ge *et al.*, 2015); Haladala layered gabbro (Long *et al.*, 2012; He *et al.*, 2016). Fields of MORB and OIB are after the compilations of Huang *et al.* (2012)

磁铁矿床钒钛磁铁矿中 V 含量(V_2O_3 = 0.45% ~ 0.93%；Liu *et al.*, 2015)。

4 岩石成因与富铁机制

4.1 后期蚀变与地壳混染

所研究样品有不同程度的蚀变现象，如单斜辉石的绿泥石化和碳酸盐化，斜长石的绢云母化和泥化等，因而全岩地球化学成分具有较高的烧失量(4.00% ~ 6.73%)。这说明岩浆后期热液蚀变对全岩主量和易活动性元素有较明显的影响，如 CaO、Rb、Ba 等含量均与 LOI 存在明显的相关性(图 6a-c)，但 $Mg^{\#}$、Sr、REE 及高场强元素等非活动性元素受蚀变作用的影响不大(图 6d-g)，仍可以反映岩浆成分特征。另外，样品 Sr-Nd 同位素组成与 LOI 并没有明显的协变关系(图 6h-i)，表明样品较大的 Sr 同位素变化并非蚀变作用结果。由于 MORB、OIB 等地幔成因基性岩与地壳组分具有显著不同的 Nb/U 和 Nb/Ta (Sun and McDonough, 1989; Rudnick and Gao, 2003)，并且所研究样品的 $^{87}Sr/^{86}Sr$ 初始比值与 Nb/U、Nb/Ta 显示出明显的负相关关系(图略)，表明其 Sr 同位素变化主要由地壳混染造成。小哈拉军山辉长岩中存在 2322 ~ 840Ma 的继承锆石年龄，暗示其形成过程中可能存在前寒武纪变质基底的混染作用。伊犁-中天山前寒武纪花岗片麻岩具有很高的 $(^{87}Sr/^{86}Sr)_i$(平均值为 ~ 0.7223; Long *et al.*, 2011; Xiong *et al.*, 2019)，但是小哈拉军山辉长岩大部分样品的 $(^{87}Sr/^{86}Sr)_i$ 较低，最低值接近于原始地幔值(0.7045，图 5)，表明其所受的地壳混染程度并不高。同样地，样品的 Nb/La 比值变化小(0.51 ~ 0.58)，但是 Nb/Ta 比值(17.1 ~ 19.6)明显高于地壳值(平均地壳 11.4; Rudnick and Gao, 2003)，也表明其所受的地壳混染程度较小。因此，本文所获得的全岩地球化学组成可用于探讨其原始岩浆性质。

4.2 岩浆结晶分异

小哈拉军山辉长岩的矿物成分显示相对演化的特征，如单斜辉石和角闪石的 $Mg^{\#}$ 较低(分别为 71 ~ 76 和 53 ~ 68)，斜长石的 An 牌号较低(20 ~ 69，表 6)。根据矿物接触关系，辉长岩呈辉绿结构，部分斜长石呈粗粒自形柱状晶体，角闪石、单斜辉石和钛磁铁矿充填于细粒自形柱状斜长石的矿物间隙(图 2)，表明斜长石最先结晶。钛磁铁矿主要充填于其他矿物间隙，其次为角闪石包裹体，少量为单斜辉石包裹体(图 2)。以上矿物形态和接触关系表明钛磁铁矿和单斜辉

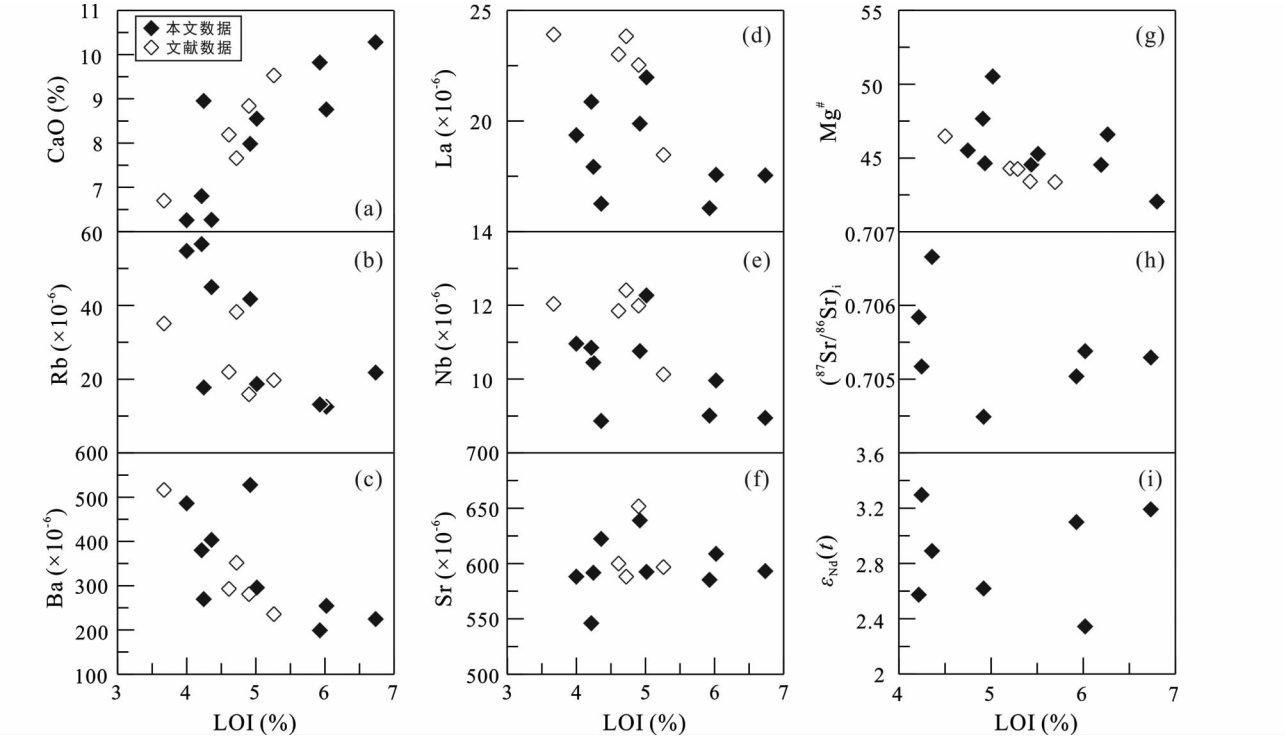


图 6 小哈拉军山辉长岩蚀变对全岩元素及同位素影响图解

Fig. 6 The diagrams of whole-rock elements and isotopes versus loss on ignition (LOI) for the Xiaohalajunshan gabbro

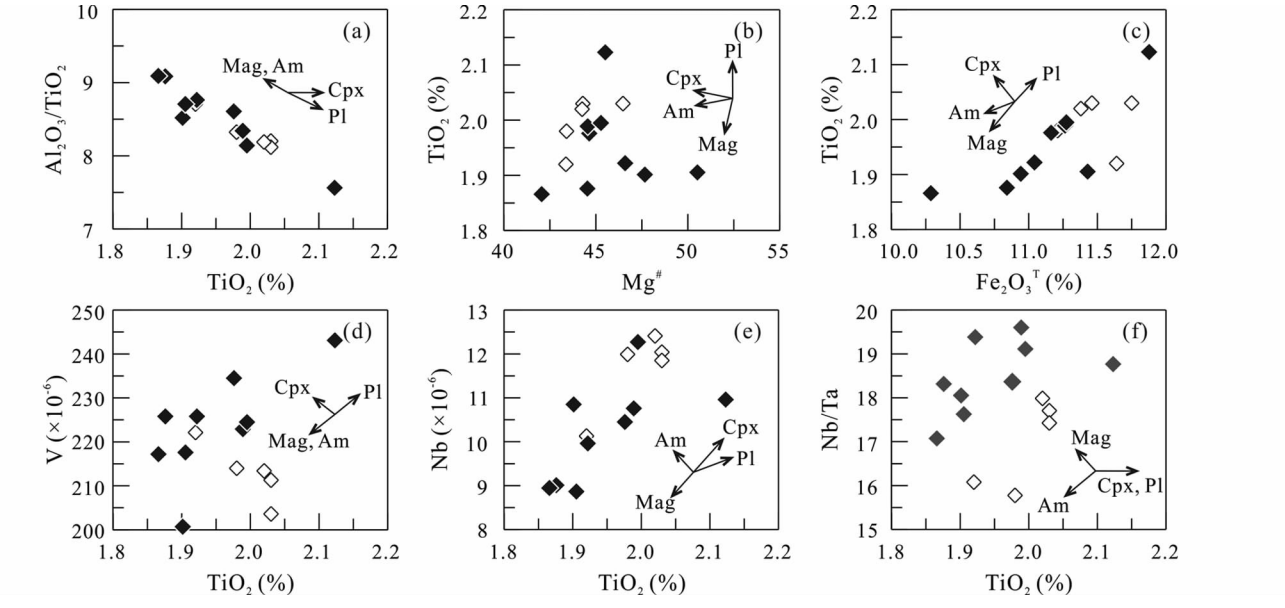


图 7 小哈拉军山辉长岩成分受结晶分异影响图解

箭头表示根据 https://earthref.org/KDD/中分配系数计算获得的矿物结晶分异后残余熔体演化趋势. 图例和数据来源同图 6

Fig. 7 The binary diagrams show the effect of fractional crystallization on whole-rock elemental compositions of the Xiaohalajunshan gabbros

Direction of arrow represents melt evolution after mineral fractionation, roughly calculated using mineral-melt partition coefficients in https://earthref.org/KDD/. Symbols and data sources are the same as in Fig. 6

石结晶早于角闪石。虽然斜长石最先结晶,但样品的全岩稀土元素配分曲线并未显示明显的 Eu 异常(δEu = 0.98 ~ 1.06),其原因可能包括两方面:(1)辉长岩的形成过程中并没有明显的斜长石结晶分异;(2)岩浆氧逸度较高,Eu 主要

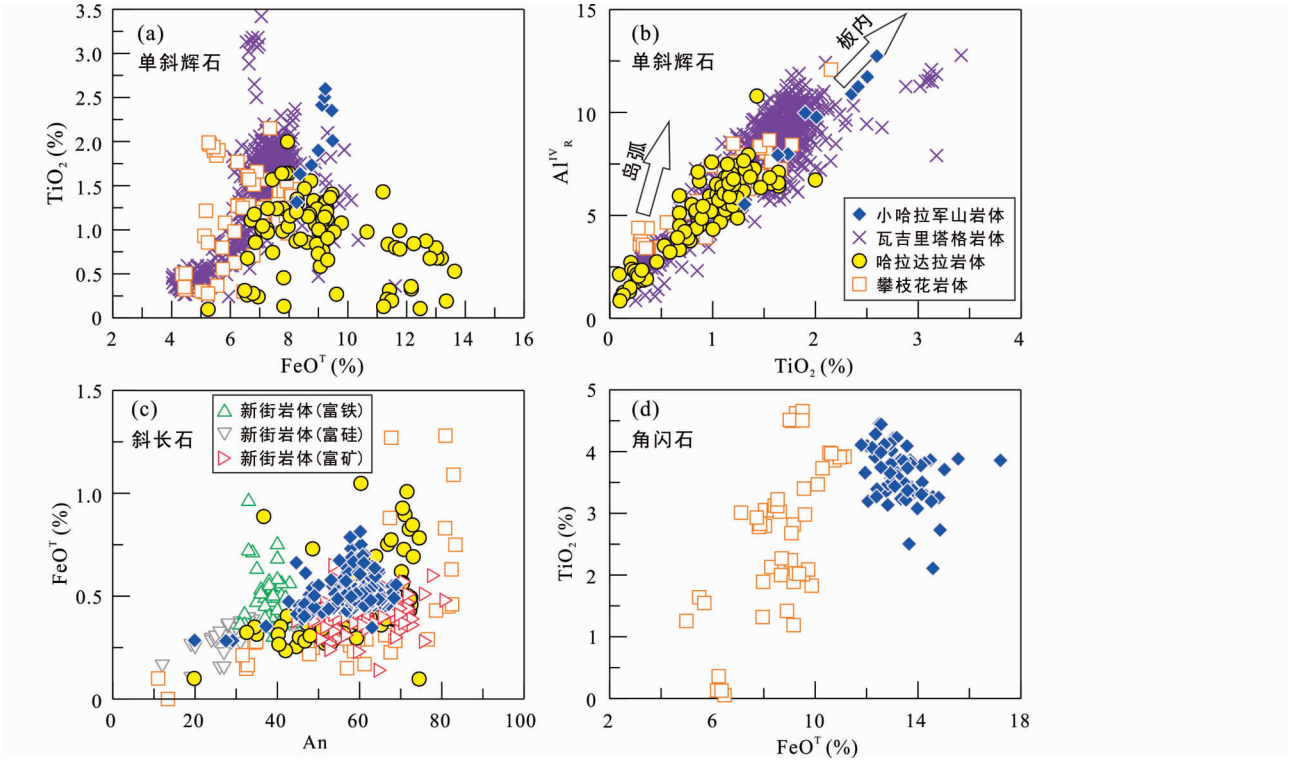


图 8　小哈拉军山辉长岩主要矿物成分变化

(a、b)单斜辉石 TiO_2 对 FeO^T 和 Al_R^{IV}；(c)斜长石 An-FeO^T；(d)角闪石 FeO^T-TiO_2. 各岩体的文献数据来源：新街岩体(董欢，2016)；瓦吉里塔格岩体(Li *et al.*，2012；Cao *et al.*，2014；Wei *et al.*，2014，2015)；哈拉达拉岩体(He *et al.*，2016)；攀枝花岩体(Gao *et al.*，2017；Tang *et al.*，2017；Wang *et al.*，2018)

Fig. 8　The compositional variation of main minerals from the Xiaohalajunshan gabbro

(a, b) TiO_2 vs. FeO^T and Al_R^{IV} of clinopyroxene; (c) An vs. FeO^T of plagioclase; (d) FeO^T vs. TiO_2 of amphibole. Literature data of all intrusions: Xinjie (Dong, 2016); Wajilitage (Li *et al.*, 2012; Cao *et al.*, 2014; Wei *et al.*, 2014, 2015); Haladala (He *et al.*, 2016); Panzhihua (Gao *et al.*, 2017; Tang *et al.*, 2017; Wang *et al.*, 2018)

以 3^+ 的形式存在，因而在斜长石-熔体的分配系数较低，即使发生斜长石的结晶分异也不会导致全岩体系出现明显的 Eu 异常(Aigner-Torres *et al.*，2007)。实验岩石学表明，在玄武质岩浆体系，当氧逸度接近于大气值时，斜长石中 Eu 的分配系数与其他 REE 相近(Aigner-Torres *et al.*，2007)。由小哈拉军山辉长岩的角闪石成分获得的氧逸度为 NNO ~ NNO + 1(表 5)，与岛弧玄武岩接近。但是，相对较早期结晶的单斜辉石中 $Mg^{\#}$ 与 Fe^{2+}/Fe^T 比值呈正相关(表 4)，反映随着岩浆演化，单斜辉石 Fe^{2+}/Fe^T 比值降低，岩浆氧逸度升高。因此，早期岩浆的氧逸度应显著低于角闪石计算的晚期岩浆氧逸度，表明早期岩浆体系为相对还原条件。实际上，钛磁铁矿主要充填于其他矿物间隙，作为包裹体主要出现在相对晚结晶的角闪石、单斜辉石以及粗粒斜长石的边部，这些特征也表明岩浆氧逸度在早期演化过程中相对较低，直至演化晚期才升高。因此，辉长岩无明显 Eu 异常现象应归因于岩浆演化过程中没有发生明显的斜长石结晶分异作用，其全岩主微量元素及其比值的二元图解所显示出来的成分变化主要是单斜辉石、钛磁铁矿和角闪石结晶分异的综合结果(图 7)。角闪石和钛磁铁矿均富集 Fe、Ti 和 V，因此岩浆中 Fe、Ti 和 V 含量主要由角闪石和钛磁铁矿的结晶分异过程控制(图 7)。随着 $Mg^{\#}$ 降低，全岩 TiO_2 呈两种趋势降低(图 7b)，主要是由于 Ti 在钛磁铁矿-熔体中分配系数大于角闪石-熔体体系，因此分别指示钛磁铁矿和角闪石的结晶分异趋势。小哈拉军山辉长岩主要矿物中只有钛磁铁矿富集 Nb(Klemme *et al.*，2006；John *et al.*，2011；Xiong *et al.*，2011)，因此随着 TiO_2 和 Nb 含量呈正相关关系主要反映了钛磁铁矿的结晶分异作用(图 7e)。小哈拉军山辉长岩具有较高的 Nb/Ta 反映岩浆源区可能有金红石残留，而角闪石的结晶分异是全岩 Nb/Ta 随着 TiO_2 含量的降低而降低的主要因素(图 7f)。

4.3　富 Fe-Ti 早期岩浆

小哈拉军山辉长岩富集钛磁铁矿(达 8% 以上；图 2)，全岩具有较高的 $Fe_2O_3^T$(10.29% ~ 11.88%)、TiO_2(1.87% ~ 2.12%)和 V(200×10^{-6} ~ 243×10^{-6})含量，可能为结晶分异导致岩浆 Fe、Ti 含量增加的结果，也可能为富 Fe、Ti 地幔源区部分熔融产生了富 Fe、Ti 岩浆。由于钛磁铁矿结晶晚于斜长石，因此斜长石中 Fe 含量随 An 变化的特征很好地反

映了钛磁铁矿结晶前岩浆中 Fe 含量的变化规律。斜长石中 Fe 含量取决于 Fe 的分配系数,而 Fe 的分配系数与岩浆 SiO_2 含量呈正相关(Lundgaard and Tegner, 2004)。由于样品的 SiO_2 变化很小,岩浆氧逸度也变化较小,表明其岩浆演化过程中的斜长石-岩浆的 Fe 分配系数基本保持不变,斜长石中 FeO^T 随 An 降低而降低的特征(图 8c)反映了斜长石演化过程中岩浆 FeO^T 含量降低的变化趋势。因此,辉长岩的早期岩浆就具有高 Fe-Ti 含量,并不是由于贫 Fe-Ti 矿物(橄榄石、斜长石等)的结晶分异造成了岩浆体系的 Fe-Ti 含量逐渐升高。另外,与塔里木大火成岩省(瓦吉里塔格岩体、哈拉达拉岩体)和峨眉山大火成岩省(攀枝花岩体、新街岩体)中富 Fe-Ti(-V)氧化物矿层状镁铁-超镁铁质岩体相比,小哈拉军山辉长岩的主要造岩矿物均具有较高的 FeO^T 和 TiO_2(图 8):(1)与哈拉达拉含钒钛磁铁矿层状辉长岩和攀枝花富 Fe-Ti-V 氧化物矿层状基性-超基性岩体中的单斜辉石(He *et al.*, 2016; Gao *et al.*, 2017; Tang *et al.*, 2017; Wang *et al.*, 2018)相比,小哈拉军山辉长岩的单斜辉石具有更高的 Fe、Ti 含量;与瓦吉里塔格富 Fe-Ti-V 氧化物矿的层状基性-超基性岩体的单斜辉石(Li *et al.*, 2012; Cao *et al.*, 2014; Wei *et al.*, 2014, 2015)相比,小哈拉军山辉长岩的单斜辉石在相同 Fe 含量时显示出更高的 Ti 含量(图 8a, b);(2)斜长石也表现出具有和其他富 Fe-Ti-V 氧化物矿基性-超基性岩体相似的 Fe 含量,而明显高于攀枝花新街岩体富硅贫矿样品中斜长石的 Fe 含量(董欢, 2016)(图 8c);(3)角闪石比攀枝花富矿样品中的角闪石(Gao *et al.*, 2017; Tang *et al.*, 2017; Wang *et al.*, 2018)具有更高的 Fe 含量(图 8d)。因此,岩相学、全岩地球化学及矿物成分特征均显示小哈拉军山辉长岩的岩浆具有富 Fe、Ti 的特征,为富 Fe、Ti 的地幔源区部分熔融形成的富 Fe、Ti 岩浆。

5 西天山早二叠世岩浆活动的构造环境

前人对天山晚石炭世-二叠纪岩浆活动的构造环境存在很大争议,主要包括俯冲构造体系与碰撞后伸展构造的两种认识。部分学者认为晚石炭世-二叠纪仍处于板块俯冲阶段,该时期的岩浆活动与俯冲体系有关(毛启贵等, 2006; Ao *et al.*, 2010; Xiao *et al.*, 2013);另有部分学者认为西天山地区的板块俯冲在晚石炭世已经结束,二叠纪的岩浆活动属于碰撞后伸展阶段的产物(Gao *et al.*, 2011; Long *et al.*, 2011; Gou *et al.*, 2012; Liu *et al.*, 2016; Xia *et al.*, 2016),研究区这一时间段的花岗岩类多为板内 A 型花岗岩(Zhang and Zou, 2013b; Li *et al.*, 2015),基性岩浆岩的 Nb-Ta-Ti 负异常等岛弧特征继承自先前俯冲板片脱水交代的地幔特征(Yan *et al.*, 2015; Liu *et al.*, 2016)。

小哈拉军山辉长岩的微量元素含量显著高于 E-MORB(图 4),并且 Sr-Nd 同位素相对富集,表明其可能形成于富集的地幔源区。辉长岩具有显著的 Nb-Ta 负异常(Nb/La = 0.51 ~ 0.58),但 Nb/Ta 比值明显高于地壳值,并不符合地壳组分直接参与的特征。通常,岛弧岩浆、受地壳混染或者地壳组分富集影响的岩浆显示出 Nb-Ta 和 Ti 的协同亏损现象。小哈拉军山辉长岩的微量元素蛛网图显示出明显的 Nb-Ta 负异常,但没有明显的 Ti 异常特征(图 4b)。虽然 Nb、Ta 常赋存于富 Ti 矿物(如金红石、钛铁矿等)(Klemme *et al.*, 2006; Gao *et al.*, 2007; John *et al.*, 2011; Xiong *et al.*, 2011),但钛磁铁矿对 Nb、Ta 的携带能力有限(He *et al.*, 2016)。小哈拉军山辉长岩富含钛磁铁矿,很可能补偿了 Ti,从而导致全岩体系的 Nb-Ta 和 Ti 地球化学行为发生解耦。虽然小哈拉军山辉长岩具有明显的俯冲流体交代特征,如 Nb-Ta 负异常、富集大离子亲石元素(图 4)等,但并不属于俯冲带岛弧岩浆活动,主要原因如下:(a)斜长石早于单斜辉石和角闪石结晶,为早期结晶矿物,并且在岩浆演化后期相对富集钛磁铁矿,表明其母岩浆并不富水,并具有较低的氧逸度(Gaetani *et al.*, 1993; Toplis and Carroll, 1995);(b)根据角闪石成分利用 Ridolfi *et al.* (2010)的方法计算获得的平衡岩浆水含量为 2.9% ~ 5.9%,接近于岛弧岩浆的水含量(2% ~ 7%);但角闪石为岩浆演化晚期结晶产物,由于岩浆演化过程中随着无水矿物的结晶会导致体系的水含量不断升高,早期岩浆的水含量理应更低;(c)岛弧基性岩浆与板内岩浆形成的单斜辉石存在明显的成分差异,例如,岛弧岩浆的富水、高氧逸度条件导致 Al 主要以 $^{\text{VI}}Mg^{\text{IV}}Si \leftrightarrow {}^{\text{VI}}Fe^{3+}{}^{\text{IV}}Al$ 的置换形式进入单斜辉石,而板内非造山拉张环境形成的基性岩浆岩中,Al 主要通过 $^{\text{VI}}Mg^{\text{IV}}Si_2 \leftrightarrow {}^{\text{VI}}Ti^{\text{IV}}Al_2$ 的置换形式进入单斜辉石,因此单斜辉石中四次配位阳离子含量(Al_R^{IV})与其 TiO_2 含量的比值可以明显区别岛弧和板内基性岩浆形成的单斜辉石(Loucks, 1990);小哈拉军山辉长岩中的单斜辉石的 Al_R^{IV} 与 TiO_2 之间的变化趋势与其他板内岩浆形成的单斜辉石相似,而明显区别于岛弧岩浆体系形成的单斜辉石(图 8b)。因此,小哈拉军山辉长岩明显区别于岛弧岩浆,应为碰撞后伸展构造环境的基性岩浆活动。

小哈拉军山辉长岩位于哈拉达拉层状辉长岩体南部约 10km 处,二者成岩年龄相近,均具有富钛磁铁矿的岩相学特征,原始岩浆的水含量和氧逸度均较低(高纪璞等, 1991; He *et al.*, 2016),因此,二者具有相似的岩浆源区和构造背景,可能属于同期的富 Fe-Ti 基性岩浆演化的结果。详细的岩石学和地球化学研究表明,哈拉达拉含磁铁矿层状辉长岩具有明显的地幔柱岩浆活动的特征,很可能是塔里木地幔柱在天山造山带这一构造薄弱带的早期岩浆活动(He *et al.*, 2016)。小哈拉军山辉长岩并非形成于单纯的碰撞后伸展作用:(a)碰撞后岩浆由于熔融程度较低且经历强烈的地壳混染作用,一般为富 K、低 Na 的岩浆(中-高 K 钙碱性-粗玄岩-超钾质岩系列;Bonin, 2004),而该辉长岩虽然为中-高 K 钙碱性岩浆,却具有较低的 K_2O/Na_2O 比值;(b)碰撞后伸展形成的岩浆活动熔融程度低,规模较小,但区域航磁异常显示特克斯的哈拉达拉和小哈拉军山基性岩体仅位于异常区东

南角(高纪璞等, 1991),小哈拉军山辉长岩和约 25km^2 的哈拉达拉层状岩体均未见较原始的矿物(如高 Fo 橄榄石或高 Mg$^{\#}$辉石等)和岩石类型(He *et al.*, 2016),表明该区域深部可能存在更大规模的隐伏岩体;(c)V-Ti 磁铁矿化的镁铁-超镁铁质岩体通常与地幔柱活动密切相关(Pirajno, 2000; 徐义刚等, 2013)。因此,小哈拉军山辉长岩很可能也是塔里木早二叠世地幔柱活动产物。西天山早二叠世广泛分布双峰式岩墙、A 型花岗岩、玄武岩和基性侵入岩,酸性岩高的锆饱和温度,以及高压-超高压变质岩的分布均表明西天山早二叠世受到塔里木地幔柱的作用(Liu *et al.*, 2013; Zhang and Zou, 2013a, b; Zhang *et al.*, 2014; Han *et al.*, 2019)。实际上,如果西天山地区在早二叠世已处于造山碰撞后的伸展阶段(Gao *et al.*, 2011; Long *et al.*, 2011; Gou *et al.*, 2012; Liu *et al.*, 2016; Xia *et al.*, 2016),将成为塔里木大火成岩省范围内地幔柱活动最易于表现和优先表现出来的地区(He *et al.*, 2016)。另外,前人研究表明,塔里木大火成岩省岩浆活动时间为 270 ~ 300Ma(Xu *et al.*, 2014),因此,形成于 295Ma 的小哈拉军山辉长岩很可能也是塔里木地幔柱在西天山的岩浆活动产物,其地幔源区在造山带闭合之前实际上为受大洋板片俯冲的地幔楔。在板片俯冲过程中,一方面地幔楔因受俯冲流体及沉积物组分的交代富集而易于熔融产生弧岩浆,另一方面俯冲的大洋板片可能会部分以辉石岩或榴辉岩的形式滞留于地幔楔,这可能也是该地区晚石炭世火山沉积岩普遍发育铁矿床重要原因。造山带闭合之后,地幔柱活动的叠加作用可能也促进了前造山带之下的富辉石岩地幔源区发生较大程度部分熔融,因而形成的哈拉达拉与小哈拉军山辉长岩同时显示出俯冲流体交代的微量元素组成特征和富集 Fe-Ti 等元素的特征。

6 结论

对西天山小哈拉军山辉长岩系统的矿物学、岩石学、地球化学和年代学研究获得以下几点认识:

(1)小哈拉军山辉长岩形成于 295 ± 3Ma,全岩富集大离子亲石元素和轻稀土元素,相对亏损的重稀土和高场强元素(Nb-Ta),Nd 同位素略亏损,Sr 同位素略富集,形成于造山带前俯冲板片交代富集的地幔源区。

(2)小哈拉军山辉长岩的具有富 Fe-Ti 的原始岩浆,并且早期岩浆的水含量和氧逸度相对较低。

(3)小哈拉军山辉长岩与相邻的哈拉达拉富 V-Ti 磁铁矿层状辉长岩具有相似的岩浆源区和矿化特征,可能都是塔里木早二叠世地幔柱在西天山造山带这一构造薄弱带的岩浆活动表现。

致谢 感谢在样品处理和实验过程中给予大力支持的王鑫玉、涂湘林、胡光黔、马金龙、夏小平等老师。李永军教授和另外两位审稿人认真评阅本文并提出了宝贵修改意见,谨致谢忱。

References

Aigner-Torres M, Blundy J, Ulmer P and Pettke T. 2007. Laser Ablation ICPMS study of trace element partitioning between plagioclase and basaltic melts: An experimental approach. Contributions to Mineralogy and Petrology, 153(6): 647 – 667

Alexeiev DV, Biske YS, Djenchuraeva AV, Kröner A and Getman OF. 2019. Late Carboniferous (Kasimovian) closure of the South Tianshan Ocean: No Triassic subduction. Journal of Asian Earth Sciences, 173: 54 – 60

Allen MB, Windley BF and Chi Z. 1993. Palaeozoic collisional tectonics and magmatism of the Chinese Tien Shan, central Asia. Tectonophysics, 220(1 – 4): 89 – 115

Ao SJ, Xiao WJ, Han CM, Mao QG and Zhang JE. 2010. Geochronology and geochemistry of Early Permian mafic-ultramafic complexes in the Beishan area, Xinjiang, NW China: Implications for Late Paleozoic tectonic evolution of the southern Altaids. Gondwana Research, 18(2 – 3): 466 – 478

Biske YS and Seltmann R. 2010. Paleozoic Tian-Shan as a transitional region between the Rheic and Urals-Turkestan oceans. Gondwana Research, 17(2 – 3): 602 – 613

Bonin B. 2004. Do coeval mafic and felsic magmas in post-collisional to within-plate regimes necessarily imply two contrasting, mantle and crustal, sources? A review. Lithos, 78(1 – 2): 1 – 24

Cao J, Wang CY, Xing CM and Xu YG. 2014. Origin of the Early Permian Wajilitag igneous complex and associated Fe-Ti oxide mineralization in the Tarim large igneous province, NW China. Journal of Asian Earth Sciences, 84: 51 – 68

Cawood PA, Kröner A, Collins WJ, Kusky TM, Mooney WD and Windley BF. 2009. Accretionary orogens through Earth history. In: Cawood PA and Kröner A (eds.). Earth Accretionary Systems in Space and Time. Geological Society, London, Special Publications, 318(1): 1 – 36

Charvet J, Shu LS and Laurent-Charvet S. 2007. Paleozoic structural and geodynamic evolution of eastern Tianshan (NW China): Welding of the Tarim and Junggar plates. Episodes, 30(3): 162 – 186

Dong H. 2016. Silicate liquid immiscibility in layered intrusion: Evidence from late-stage microstructure and mineral composition. Ph. D. Dissertation. Beijing: University of Chinese Academy of Sciences, 121 – 157 (in Chinese with English summary)

Gaetani GA, Grove TL and Bryan WB. 1993. The influence of water on the petrogenesis of subductionrelated igneous rocks. Nature, 365(6444): 332 – 334

Gao J, John T, Klemd R and Xiong XM. 2007. Mobilization of Ti-Nb-Ta during subduction: Evidence from rutile-bearing dehydration segregations and veins hosted in eclogite, Tianshan, NW China. Geochimica et Cosmochimica Acta, 71(20): 4974 – 4996

Gao J, Long LL, Klemd R, Qian Q, Liu DY, Xiong XM, Su W, Liu W, Wang YT and Yang FQ. 2009. Tectonic evolution of the South Tianshan orogen and adjacent regions, NW China: Geochemical and age constraints of granitoid rocks. International Journal of Earth Sciences, 98(6): 1221 – 1238

Gao J, Klemd R, Qian Q, Zhang X, Li JL, Jiang T and Yang YQ. 2011. The collision between the Yili and Tarim blocks of the southwestern Altaids: Geochemical and age constraints of a leucogranite dike crosscutting the HP-LT metamorphic belt in the Chinese Tianshan Orogen. Tectonophysics, 499(1 – 4): 118 – 131

Gao J, Wang XS, Klemd R, Jiang T, Qian Q, Mu LX and Ma YZ. 2015. Record of assembly and breakup of Rodinia in the southwestern Altaids: Evidence from Neoproterozoic magmatism in the Chinese Western Tianshan Orogen. Journal of Asian Earth Sciences, 113: 173 – 193

Gao JP, Li XZ, Yang HQ, Luo YP and Yao WG. 1991. A study on the geological characteristics and ore-finding prospects of Tekes basic

body in Xinjiang. Northwest Geoscience, (3): 95 - 144 (in Chinese with English abstract)

Gao WY, Ciobanu CL, Cook NJ, Huang F, Meng L and Gao S. 2017. Petrography and trace element signatures in silicates and Fe-Ti-oxides from the Lanjiahuoshan deposit, Panzhihua layered intrusion, Southwest China. Lithos, 294 - 295: 164 - 183

Gao YW, Wang ZH, Zhang ZL, Li ZY, Dong FC, Tan WJ and Jiang HB. 2017. Geochemical characteristics of volcanic rocks in Kuolasayi iron deposit, western Tianshan and its geological and metallogenic significance. Geological Science and Technology Information, 36(4): 10 - 18 (in Chinese with English abstract)

Ge SS, Zhai MG, Safonova I, Li DP, Zhu XY, Zuo PF and Shan HX. 2015. Whole-rock geochemistry and Sr-Nd-Pb isotope systematics of the Late Carboniferous volcanic rocks of the Awulale metallogenic belt in the western Tianshan Mountains (NW China): Petrogenesis and geodynamical implications. Lithos, 228 - 229: 62 - 77

Gou LL, Zhang LF, Tao RB and Du JX. 2012. A geochemical study of syn-subduction and post-collisional granitoids at Muzhaerte River in the Southwest Tianshan UHP belt, NW China. Lithos, 136 - 139: 201 - 224

Guo X and Zhu YF. 2011. Petrologic and geochemical research of Xiaohalajunshan gabbro in Southwest Tianshan Mts., Xinjiang. Earth Science Frontiers, 18(2): 180 - 190 (in Chinese with English abstract)

Han BF, Guo ZJ, Zhang ZC, Zhang L, Chen JF and Song B. 2010. Age, geochemistry, and tectonic implications of a Late Paleozoic stitching pluton in the North Tian Shan suture zone, western China. GSA Bulletin, 122(3 - 4): 627 - 640

Han BF, He GQ, Wang XC and Guo ZJ. 2011. Late Carboniferous collision between the Tarim and Kazakhstan-Yili terranes in the western segment of the South Tian Shan Orogen, Central Asia, and implications for the Northern Xinjiang, western China. Earth-Science Reviews, 109(3 - 4): 74 - 93

Han YG and Zhao GC. 2018. Final amalgamation of the Tianshan and Junggar orogenic collage in the southwestern Central Asian Orogenic Belt: Constraints on the closure of the Paleo-Asian Ocean. Earth-Science Reviews, 186: 129 - 152

Han YG, Zhao GC, Cawood PA, Sun M, Liu Q and Yao JL. 2019. Plume-modified collision orogeny: The Tarim-western Tianshan example in Central Asia. Geology, 47(10): 1001 - 1005

He PL, Huang XL, Li HY, Li J, Yu Y and Li WX. 2013. Mechanism of Fe-Ti enrichment in the Haladala gabbros: Implication for the tectonic evolution of the western Tianshan orogenic belt. Acta Petrologica Sinica, 29(10): 3457 - 3472 (in Chinese with English abstract)

He PL, Huang XL, Xu YG, Li HY, Wang X and Li WX. 2016. Plume-orogenic lithosphere interaction recorded in the Haladala layered intrusion in the Southwest Tianshan Orogen, NW China. Journal of Geophysical Research, 121(3): 1525 - 1545

He ZY, Klemd R, Zhang ZM, Zong KQ, Sun LX, Tian ZL and Huang BT. 2015. Mesoproterozoic continental arc magmatism and crustal growth in the eastern Central Tianshan Arc Terrane of the southern Central Asian Orogenic Belt: Geochronological and geochemical evidence. Lithos, 236 - 237: 74 - 89

Huang XL, Zhong JW and Xu YG. 2012. Two tales of the continental lithospheric mantle prior to the destruction of the North China Craton: Insights from Early Cretaceous mafic intrusions in western Shandong, East China. Geochimica et Cosmochimica Acta, 96: 193 - 214

Huang ZY, Long XP, Yuan C, Sun M, Wang YJ, Zhang YY and Chen B. 2016. Detrital zircons from Neoproterozoic sedimentary rocks in the Yili Block: Constraints on the affinity of microcontinents in the southern Central Asian Orogenic Belt. Gondwana Research, 37: 39 - 52

Jahn BM, Wang T and Litvinovsky BA. 2006. Crustal growth in the Central Asian orogenic belt (the Altaids): Nd isotope evidence. Geochimica et Cosmochimica Acta, 70(18S): A287

John T, Klemd R, Klemme S, Pfänder JA, Hoffmann JE and Gao J. 2011. Nb-Ta fractionation by partial melting at the titanite-rutile transition. Contributions to Mineralogy and Petrology, 161(1): 35 - 45

Klemd R, Gao J, Li JL and Meyer M. 2015. Metamorphic evolution of (ultra)-high-pressure subduction-related transient crust in the South Tianshan Orogen (Central Asian Orogenic Belt): Geodynamic implications. Gondwana Research, 28(1): 1 - 25

Klemme S, Günther D, Hametner K, Prowatke S and Zack T. 2006. The partitioning of trace elements between ilmenite, ulvospinel, armalcolite and silicate melts with implications for the early differentiation of the moon. Chemical Geology, 234(3 - 4): 251 - 263

Kröner A, Kovach V, Alexeiev D, Wang KL, Wong J, Degtyarev K and Kozakov I. 2017. No excessive crustal growth in the Central Asian Orogenic Belt: Further evidence from field relationships and isotopic data. Geodynamics & Tectonophysics, 8(3): 503 - 504

Li NB, Niu HC, Shan Q and Yang WB. 2015. Two episodes of Late Paleozoic A-type magmatism in the Qunjisayi area, western Tianshan: Petrogenesis and tectonic implications. Journal of Asian Earth Sciences, 113: 238 - 253

Li XH, Li WX, Li QL, Wang XC, Liu Y and Yang YH. 2010. Petrogenesis and tectonic significance of the ~850Ma Gangbian alkaline complex in South China: Evidence from in situ zircon U-Pb dating, Hf-O isotopes and whole-rock geochemistry. Lithos, 114(1 - 2): 1 - 15

Li XH, Tang GQ, Gong B, Yang YH, Hou KJ, Hu ZC, Li QL, Liu Y and Li WX. 2013. Qinghu zircon: A working reference for microbeam analysis of U-Pb age and Hf and O isotopes. Chinese Science Bulletin, 58(36): 4647 - 4654

Li YJ, Xu Q, Yang GX, Wang R, Tong LL, Li GY, Shen R, Li Z, Wang ZP and Wang ZY. 2018. Carboniferous tectonic configuration of the Yining Massif in Western Tianshan, NW China. Geological Journal, 53(S2): 60 - 75

Li YQ, Li ZL, Chen HL, Yang SF and Yu X. 2012. Mineral characteristics and metallogenesis of the Wajilitag layered mafic-ultramafic intrusion and associated Fe-Ti-V oxide deposit in the Tarim large igneous province, Northwest China. Journal of Asian Earth Sciences, 49: 161 - 174

Liu HQ, Xu YG and He B. 2013. Implications from zircon-saturation temperatures and lithological assemblages for Early Permian thermal anomaly in Northwest China. Lithos, 182 - 183: 125 - 133

Liu HQ, Xu YG, Wei GJ, Wei JX, Yang F, Chen XY, Liu L and Wei X. 2016. B isotopes of Carboniferous-Permian volcanic rocks in the Tuha basin mirror a transition from subduction to intraplate setting in Central Asian Orogenic Belt. Journal of Geophysical Research, 121(11): 7946 - 7964

Liu PP, Zhou MF, Chen WT, Gao JF and Huang XW. 2015. In-situ LA-ICP-MS trace elemental analyses of magnetite: Fe-Ti-(V) oxide-bearing mafic-ultramafic layered intrusions of the Emeishan Large Igneous Province, SW China. Ore Geology Reviews, 65: 853 - 871

Long LL, Gao J, Xiong XM and Qian Q. 2007. Geochemistry and geochronology of granitoids in Bikai region, southern Central-Tianshan mountains, Xinjiang. Acta Petrologica Sinica, 23(4): 719 - 732 (in Chinese with English abstract)

Long LL, Gao J, Klemd R, Beier C, Qian Q, Zhang X, Wang JB and Jiang T. 2011. Geochemical and geochronological studies of granitoid rocks from the Western Tianshan Orogen: Implications for continental growth in the southwestern Central Asian Orogenic Belt. Lithos, 126(3 - 4): 321 - 340

Long LL, Wang YW, Tang PZ, Wang LJ, Wang JB and Liao Z. 2012. A debate on the special circumstance of rock-forming and ore-forming of Haladala pluton, a mafic-ultramafic complex related to CuNi-VTiFe composite mineralization, in western Tianshan. Acta Petrologica Sinica, 28(7): 2015 - 2028 (in Chinese with English abstract)

Loucks RR. 1990. Discrimination of ophiolitic from nonophiolitic ultramafic-mafic allochthons in orogenic belts by the Al/Ti Ratio in Clinopyroxene. Geology, 18(4): 346 - 349

Lundgaard KL and Tegner C. 2004. Partitioning of ferric and ferrous iron

between plagioclase and silicate melt. Contributions to Mineralogy and Petrology, 147(4): 470 – 483

Mao QG, Xiao WJ, Han CM, Sun M, Yuan C, Yan Z, Li JL, Yong Y and Zhang JE. 2006. Zircon U-Pb age and the geochemistry of the Baishiquan mafic-ultramafic complex in the eastern Tianshan, Xinjiang Province: Constraints on the closure of the Paleo-Asian Ocean. Acta Petrologica Sinica, 22(1): 153 – 162 (in Chinese with English abstract)

Mao YJ, Qin KZ and Tang DM. 2018. Revisiting the age and emplacement process of the Huangshandong Ni-Cu deposit in the Central Asian Orogenic belt, northwestern China: Implications for multiple magma extractions from a short-lived staging magma chamber. Lithos, 320 – 321: 583 – 591

Pirajno F. 2000. Ore Deposits and Mantle Plumes. London: Kluwer Academic Publisher, 1 – 556

Pouchou JL and Pichoir F. 1991. Quantitative analysis of homogeneous or stratified microvolumes applying the model "PAP". In: Heinrich KFJ and Newbury DE (eds.). Electron Probe Quantitation. Boston, MA: Springer, 31 – 75

Qian Q, Gao J, Klemd R, He GQ, Song B, Liu DY and Xu RH. 2009. Early Paleozoic tectonic evolution of the Chinese South Tianshan Orogen: Constraints from SHRIMP zircon U-Pb geochronology and geochemistry of basaltic and dioritic rocks from Xiate, NW China. International Journal of Earth Sciences, 98(3): 551 – 569

Qin KZ, Su BX, Sakyi PA, Tang DM, Li XH, Sun H, Xiao QH and Liu PP. 2011. SIMS zircon U-Pb geochronology and Sr-Nd isotopes of Ni-Cu-bearing mafic-ultramafic intrusions in Eastern Tianshan and Beishan in correlation with flood basalts in Tarim basin (NW China): Constraints on a ca. 280Ma mantle plume. American Journal of Science, 311(3): 237 – 260

Ren MH, Wang Y, Ni K and Sun YL. 2013. Differentiation of magmas in the formation of Permian mafic-ultramafic intrusions in the Dacaotan area, Eastern Tianshan: Implications for Ni-Cu-(PGE) sulfide mineralization potentials. Acta Petrologica Sinica, 29(10): 3473 – 3486 (in Chinese with English abstract)

Ridolfi F, Renzulli A and Puerini M. 2010. Stability and chemical equilibrium of amphibole in calc-alkaline magmas: An overview, new thermobarometric formulations and application to subduction-related volcanoes. Contributions to Mineralogy and Petrology, 160(1): 45 – 66

Rudnick RL and Gao S. 2003. Composition of the continental crust. Treatise on Geochemistry, 3: 1 – 64

Şengör AMC, Natal'in BA and Burtman VS. 1993. Evolution of the altaid tectonic collage and Palaeozoic crustal growth in Eurasia. Nature, 364(6435): 299 – 307

Su BX, Qin KZ, Tang DM, Sakyi PA, Liu PP, Sun H and Xiao QH. 2013. Late Paleozoic mafic-ultramafic intrusions in southern Central Asian Orogenic Belt (NW China): Insight into magmatic Ni-Cu sulfide mineralization in orogenic setting. Ore Geology Reviews, 51: 57 – 73

Su BX, Qin KZ, Lu YH, Sun H and Sakyi PA. 2015. Decoupling of whole-rock Nd-Hf and zircon Hf-O isotopic compositions of a 284Ma mafic-ultramafic intrusion in the Beishan Terrane, NW China. International Journal of Earth Sciences, 104(7): 1721 – 1737

Sun SS and McDonough WF. 1989. Chemical and isotopic systematics of oceanic basalts: Implications for mantle composition and processes. In: Saunders AD and Norry (eds.). Magmatism in the Ocean Basins. Geological Society, London, Special Publications, 42(1): 313 – 345

Tanaka T, Togashi S, Kamioka H, Amakawa H, Kagami H, Hamamoto T, Yuhara M, Orihashi Y, Yoneda S, Shimizu H, Kunimaru T, Takahashi K, Yanagi T, Nakano T, Fujimaki H, Shinjo R, Asahara Y, Tanimizu M and Dragusanu C. 2000. Jndi-1: A neodymium isotopic reference in consistency with LaJolla neodymium. Chemical Geology, 168(3 – 4): 279 – 281

Tang QY, Li CS, Tao Y, Ripley EM and Xiong F. 2017. Association of Mg-rich olivine with magnetite as a result of brucite marble assimilation by basaltic magma in the Emeishan Large Igneous Province, SW China. Journal of Petrology, 58(4): 699 – 714

Tong LL, Li YJ, Li GY, Li ZC, Yang GX, Wang ZP, Wang ZY, Shen R and Li Z. 2018. Sr-Nd isotopes of Early and Late Carboniferous volcanic rocks in Yining Massif (Xinjiang, NW China): Implications for petrogenesis and tectonic evolution of western Tianshan. Geological Journal, 53(S2): 137 – 147

Toplis MJ and Carroll MR. 1995. An experimental study of the influence of oxygen fugacity on Fe-Ti oxide stability, phase relations, and mineral-melt equilibria in ferro-basaltic systems. Journal of Petrology, 36(5): 1137 – 1170

Wang B, Shu LS, Faure M, Jahn BM, Cluzel D, Charvet J, Chung SL and Meffre S. 2011. Paleozoic tectonics of the southern Chinese Tianshan: Insights from structural, chronological and geochemical studies of the Heiyingshan ophiolitic mélange (NW China). Tectonophysics, 497(1 – 4): 85 – 104

Wang K, Wang CY and Ren ZY. 2018. Apatite-hosted melt inclusions from the Panzhihua gabbroic-layered intrusion associated with a giant Fe-Ti oxide deposit in SW China: Insights for magma unmixing within a crystal mush. Contributions to Mineralogy and Petrology, 173(7): 59

Wang XS, Gao J, Klemd R, Jiang T, Li JL, Zhang X, Tan Z, Li L and Zhu ZX. 2014. Geochemistry and geochronology of the Precambrian high-grade metamorphic complex in the Southern Central Tianshan ophiolitic mélange, NW China. Precambrian Research, 254: 129 – 148

Wei X, Xu YG, Zhang CL, Zhao JX and Feng YX. 2014. Petrology and Sr-Nd isotopic disequilibrium of the Xiaohaizi intrusion, NW China: Genesis of layered intrusions in the Tarim Large Igneous Province. Journal of Petrology, 55(12): 2567 – 2598

Wei X, Xu YG, Luo ZY, Zhao JX and Feng YX. 2015. Composition of the Tarim mantle plume: Constraints from clinopyroxene antecrysts in the Early Permian Xiaohaizi dykes, NW China. Lithos, 230: 69 – 81

Windley BF, Alexeiev D, Xiao WJ, Kröner A and Badarch G. 2007. Tectonic models for accretion of the Central Asian Orogenic Belt. Journal of the Geological Society, 164(1): 31 – 47

Xia B, Zhang LF and Zhang L. 2016. Petrogenesis and tectonic implications of Permian post-collisional granitoids in the Chinese southwestern Tianshan, NW China. Journal of Asian Earth Sciences, 130: 60 – 74

Xia LQ, Xu XY, Xia ZC, Li XM, Ma ZP and Wang LS. 2004. Petrogenesis of Carboniferous rift-related volcanic rocks in the Tianshan, northwestern China. GSA Bulletin, 116(3 – 4): 419 – 433

Xiao WJ, Huang BC, Han CM, Sun S and Li JL. 2010. A review of the western part of the Altaids: A key to understanding the architecture of accretionary orogens. Gondwana Research, 18(2 – 3): 253 – 273

Xiao WJ, Windley BF, Allen MB and Han CM. 2013. Paleozoic multiple accretionary and collisional tectonics of the Chinese Tianshan orogenic collage. Gondwana Research, 23(4): 1316 – 1341

Xiao WJ and Santosh M. 2014. The western Central Asian Orogenic Belt: A window to accretionary orogenesis and continental growth. Gondwana Research, 25(4): 1429 – 1444

Xiong FH, Hou MC, Cawood PA, Huang H, Ducea MN and Ni SJ. 2019. Neoproterozoic I-type and highly fractionated A-type granites in the Yili Block, Central Asian Orogenic Belt: Petrogenesis and tectonic implications. Precambrian Research, 328: 235 – 249

Xiong XL, Keppler H, Audétat A, Ni HW, Sun WD and Li Y. 2011. Partitioning of Nb and Ta between rutile and felsic melt and the fractionation of Nb/Ta during partial melting of hydrous metabasalt. Geochimica et Cosmochimica Acta, 75(7): 1673 – 1692

Xu YG, Wang Y, Wei X and He B. 2013. Mantle plume-related mineralization and their principal controlling factors. Acta Petrologica Sinica, 29(10): 3307 – 3322 (in Chinese with English abstract)

Xu YG, Wei X, Luo ZY, Liu HQ and Cao J. 2014. The Early Permian Tarim Large Igneous Province: Main characteristics and a plume incubation model. Lithos, 204: 20 – 35

Yan S, Shan Q, Niu HC, Yang WB, Li NB, Zeng LJ and Jiang YH.

2015. Petrology and geochemistry of Late Carboniferous hornblende gabbro from the Awulale Mountains, western Tianshan (NW China): Implication for an arc-nascent back-arc environment. Journal of Asian Earth Sciences, 113: 218 – 237

Zhang CL and Zou HB. 2013a. Comparison between the Permian mafic dykes in Tarim and the western part of Central Asian Orogenic Belt (CAOB), NW China: Implications for two mantle domains of the Permian Tarim Large Igneous Province. Lithos, 174: 15 – 27

Zhang CL and Zou HB. 2013b. Permian A-type granites in Tarim and western part of Central Asian Orogenic Belt (CAOB): Genetically related to a common Permian mantle plume? Lithos, 172 – 173: 47 – 60

Zhang CL, Zou HB, Yao CY and Dong YG. 2014. Origin of Permian gabbroic intrusions in the southern margin of the Altai Orogenic belt: A possible link to the Permian Tarim mantle plume? Lithos, 204: 112 – 124

Zhang LF, Ai YL, Li XP, Rubatto D, Song B, Williams S, Song SG, Ellis D and Liou JG. 2007. Triassic collision of western Tianshan orogenic belt, China: Evidence from SHRIMP U-Pb dating of zircon from HP/UHP eclogitic rocks. Lithos, 96(1 – 2): 266 – 280

Zhang X, Tian JQ, Gao J, Klemd R, Dong LH, Fan JJ, Jiang T, Hu CJ and Qian Q. 2012. Geochronology and geochemistry of granitoid rocks from the Zhibo syngenetic volcanogenic iron ore deposit in the Western Tianshan Mountains (NW-China): Constraints on the age of mineralization and tectonic setting. Gondwana Research, 22(2): 585 – 596

Zhang X, Klemd R, Gao J, Dong LH, Wang XS, Haase K, Jiang T and Qian Q. 2015a. Metallogenesis of the Zhibo and Chagangnuoer volcanic iron oxide deposits in the Awulale Iron Metallogenic Belt, Western Tianshan orogen, China. Journal of Asian Earth Sciences, 113: 151 – 172

Zhang XR, Zhao GC, Eizenhöfer PR, Sun M, Han YG, Hou WZ, Liu DX, Wang B, Liu Q and Xu B. 2015b. Latest Carboniferous closure of the Junggar Ocean constrained by geochemical and zircon U-Pb-Hf isotopic data of granitic gneisses from the Central Tianshan block, NW China. Lithos, 238: 26 – 36

Zhu XY, Wang B, Cluzel D, He ZY, Zhou Y and Zhong L. 2019. Early Neoproterozoic gneissic granitoids in the southern Yili Block (NW China): Constraints on microcontinent provenance and assembly in the SW Central Asian Orogenic Belt. Precambrian Research, 325: 111 – 131

Zhu YF, Guo X, Song B, Zhang LF and Gu LB. 2009. Petrology, Sr-Nd-Hf isotopic geochemistry and zircon chronology of the Late Palaeozoic volcanic rocks in the southwestern Tianshan Mountains, Xinjiang, NW China. Journal of the Geological Society, 166(6): 1085 – 1099

附中文参考文献

董欢. 2016. 层状岩体中的岩浆不混熔作用: 来自显微结构和矿物成分的记录. 博士学位论文. 北京: 中国科学院大学, 121 – 157

高纪璞, 李先梓, 杨合群, 罗玉鹏, 姚文光. 1991. 新疆特克斯基性岩体地质特征及找矿方向研究. 西北地质科学, (3): 95 – 144

高永伟, 王志华, 张振亮, 李忠煜, 董福辰, 谭文娟, 姜寒冰. 2017. 西天山阔拉萨依铁矿火山岩地球化学特征及其地质矿产意义. 地质科技情报, 36(4): 10 – 18

郭璇, 朱永峰. 2011. 新疆西南天山小哈拉军山辉长岩体岩石学及地球化学研究. 地学前缘, 18(2): 180 – 190

贺鹏丽, 黄小龙, 李洪颜, 李洁, 于洋, 李武显. 2013. 西天山哈拉达拉辉长岩的 Fe-Ti 富集机制及其构造意义. 岩石学报, 29(10): 3457 – 3472

龙灵利, 高俊, 熊贤明, 钱青. 2007. 新疆中天山南缘比开(地区)花岗岩地球化学特征及年代学研究. 岩石学报, 23(4): 719 – 732

龙灵利, 王玉往, 唐萍芝, 王莉娟, 王京彬, 廖震. 2012. 西天山 CuNi-VTiFe 复合型矿化镁铁-超镁铁杂岩——哈拉达拉岩体成岩成矿背景特殊性讨论. 岩石学报, 28(7): 2015 – 2028

毛启贵, 肖文交, 韩春明, 孙敏, 袁超, 闫臻, 李继亮, 雍拥, 张继恩. 2006. 新疆东天山白石泉铜镍矿床基性-超基性岩体锆石 U-Pb 同位素年龄、地球化学特征及其对古亚洲洋闭合时限的制约. 岩石学报, 22(1): 153 – 162

任明浩, 王焰, 倪康, 孙亚莉. 2013. 东天山二叠纪大草滩地区镁铁-超镁铁质岩体的岩浆演化过程和含矿性. 岩石学报, 29(10): 3473 – 3486

徐义刚, 王焰, 位荀, 何斌. 2013. 与地幔柱有关的成矿作用及其主控因素. 岩石学报, 29(10): 3307 – 3322